https://doi.org/10.5194/egusphere-2026-3104
Preprint. Discussion started: 18 June 2026

60 years of global air-sea CO_2 flux variability

Suki C. K. Wong[1,2], Galen A. McKinley[1,2], Richard Seager[1], Tess Wei-Ping Jacobson[3], Amanda Fay[1], Özgür Gürses[4], Nicolas Gruber[5], Tatiana Ilyina[6], Tereza Jarnikova[7], Laure Resplandy[8], Jörg Schwinger[9], and Roland Séférian[10]

[1]Lamont-Doherty Earth Observatory, Columbia University, New York, USA
[2]Department of Earth and Environmental Sciences, Columbia University, New York, USA
[3]NASA Goddard Institute for Space Studies, New York, USA
[4]Alfred Wegener Institute, Helmholtz Centre for Polar and Marine Research, Germany
[5]Environmental Physics, Institute of Biogeochemistry and Pollutant Dynamics, ETH Zurich, Zürich, Switzerland.
[6]Max Planck Institute for Marine Microbiology, Bremen, Germany
[7]University of East Anglia, UK
[8]Princeton University, New Jersey, USA
[9]NORCE Climate & Bjerknes Centre for Climate Research, Bergen, Norway
[10]Centre National de Recherches Météorologiques, France

Correspondence: Suki Wong (suki.wong@columbia.edu)

Abstract. The ocean carbon sink has absorbed approximately 29% of anthropogenic carbon dioxide (CO_2) emissions in the last decade, mitigating climate change. Over time, the ocean carbon sink has grown nearly proportionally to atmospheric CO_2 concentrations. Natural variability also modulates the ocean carbon sink, but the decadal-timescale mechanisms of this variability are not well-understood. Using LDEO-Hybrid Physics Data, a unique observation-based product that merges observations with hindcast models, we assess the decadal variability of global air-sea CO_2 fluxes for 1959-2024, with a focus on the dominant regional contributions. The dominant mode of decadal air-sea CO_2 flux variability exhibits strong synchronous signals between the tropical Pacific and the Southern Ocean. This synchronicity is modulated by Pacific Decadal Variability (PDV) and the interannually varying El Niño-Southern Oscillation (ENSO) as measured by the Multivariate ENSO Index. When PDV and MEI indices are positive, the Southern Ocean experiences stronger westerly winds and deeper mixed layers. However, fully explaining the weakening of the Southern Ocean carbon sink in recent decades, which had predominantly negative PDV and MEI, will require additional constraints, particularly for biological processes.

1 Introduction

Over the industrial era, the ocean has absorbed anthropogenic carbon at a rate roughly proportional to atmospheric carbon dioxide (CO_2) concentrations, taking up approximately 30% of annual anthropogenic CO_2 emissions (Friedlingstein et al., 2025; Gruber et al., 2023). By damping the rate of atmospheric CO_2 accumulation, the ocean carbon sink has mitigated the effects of climate change. The primary driver of the increasing ocean carbon sink is the growth of atmospheric CO_2, which drives the air-sea flux of CO_2 (FCO_2) into the ocean (McKinley et al., 2020). As atmospheric CO_2 rises, the ocean carbon sink grows proportionally (Gruber et al., 2023; Müller et al., 2023). There is also substantial variability around this long-term

https://doi.org/10.5194/egusphere-2026-3104
Preprint. Discussion started: 18 June 2026

growth, due to both external and internal climate forcing (Landschützer et al., 2015; DeVries et al., 2017; Landschützer et al., 2019; McKinley et al., 2020; Gruber et al., 2023; Fay et al., 2023, 2024).

The total variability in the ocean carbon sink results from a combination of internal processes and external forcings (Crisp et al., 2022; Fay et al., 2023, 2024). The largest signal of interannual FCO_2 variability is driven by internal processes, particularly the El Niño-Southern Oscillation (ENSO) in the equatorial Pacific (Feely et al., 1999; McKinley et al., 2004; Ishii et al., 2014; Wong et al., 2022). Anomalous fluxes from the equatorial Pacific strongly influence interannual anomalies in the strength of the total global ocean sink (McKinley et al., 2004; Gruber et al., 2023).

The decadal variability of the ocean carbon sink in recent decades - in particular, the weakened sink in the 1990s and its recovery in the 2000s - has been the focus for a number of studies (Le Quéré et al., 2007; Landschützer et al., 2015, 2016; DeVries et al., 2019; Gruber et al., 2019; McKinley et al., 2020; Fay et al., 2023, 2024). McKinley et al. (2020) and Fay et al. (2024) use models with a range of complexities to demonstrate that about 50% of recent variability in the ocean carbon sink is externally driven by variations in the atmospheric growth rate. In addition, the weakening of the sink over the decade of the 1990s can be explained by a reduced atmospheric growth rate during the 1990s, punctuated by a significant increase in uptake occurring early in the decade with the global upper ocean cooling due to Mount Pinatubo's eruption in 1991. Following this, the re-warming of the surface ocean, together with the excess carbon that was absorbed post-eruption, elevated surface ocean partial pressure of CO_2 levels (pCO_2) relative to atmospheric pCO_2 causing ΔpCO_2 (ocean minus atmosphere) to become less negative, weakening the sink over the 1990s (Fay et al., 2023). Other proposed mechanisms for a weakened sink post 2000 include internally driven sea surface temperature (SST) changes which affected the solubility of CO_2 (Landschützer et al., 2016) and the intensification of westerly winds over the Southern Ocean, associated with the Southern Annular Mode, enhancing the upwelling of CO_2 (Le Quéré et al., 2007). Though the decadal variability of the global ocean carbon sink is a result of changes in all basins, decadal changes in the equatorial Pacific and the Southern Ocean appear to be quantitatively most significant (DeVries et al., 2019; Landschützer et al., 2019; Bennington et al., 2022; Gruber et al., 2023). The decadal variability of the Southern Ocean sink, which cumulatively has the largest sink for anthropogenic CO_2 when integrated over its large area (Mikaloff Fletcher et al., 2006), remains uncertain, largely due to sparse observations (Fay et al., 2014; Gloege et al., 2021; Mayot et al., 2023; Heimdal et al., 2024).

Large variability in the ocean carbon sink, compounded with the uncertainties in sink estimates, confounds the ability to identify changes in the ocean carbon sink that are due to carbon-climate feedbacks and external forcing, such as changes in emissions (Peters et al., 2017; Lovenduski et al., 2021; Friedlingstein et al., 2025). To support these efforts and to better predict the future ocean carbon sink, better quantification and a mechanistic understanding of the sink's variability is necessary (Peters et al., 2017; Crisp et al., 2022).

In order to quantify ocean sink variability, global estimates of air-sea CO_2 fluxes are needed. This requires observations of surface ocean CO_2 fugacity (fCO_2), a close cousin of the partial pressure (pCO_2). Unfortunately, available observations are extremely sparse (Bakker et al., 2016) in both space and time. To fill the observational gaps, a number of approaches have been developed to statistically extrapolate sparse fCO_2 observations to create observations-based data products of fully gridded, monthly fCO_2 estimates, which can then be used to calculate air-sea CO_2 fluxes (Gloege et al., 2022; Bennington

https://doi.org/10.5194/egusphere-2026-3104
Preprint. Discussion started: 18 June 2026

et al., 2022; Gregor et al., 2019; Denvil-Sommer et al., 2019; Rödenbeck et al., 2015). However, temporal coverage by most observations-based data products does not start until the 1980s since this is when surface ocean carbon observations began to be numerous enough for direct reconstruction. Studies of ocean carbon sink variability prior to the 1980s to date have relied on models, which come with their own set of uncertainties and biases (Deser et al., 2012a). Additionally, until 2020 the annual estimate of the global ocean carbon sink provided by the annually-updated Global Carbon Budget only included models to quantify the estimate (Friedlingstein et al., 2020). Since then, the Global Carbon Budget has incorporated both models and observations-based data products as a basis for their ocean sink estimates for 1990 onward. Only two products that submit to the Global Carbon Budget provide ocean carbon sink estimates for years prior to 1980. The addition of observations-based data products provides estimates that are independent of the models. While a convergence between models and data-based estimates indicates confidence in the understanding of the driving mechanisms, a lack of understanding can be identified through divergences between these independent estimates (Hauck et al., 2020; Friedlingstein et al., 2020).

Gloege et al. (2022) and Bennington et al. (2022) developed a global pCO_2 data product (the LDEO-Hybrid Physics Data product, LDEO-HPD) that demonstrates high skill relative to other data products. This novel approach interpolates sparse surface ocean fCO_2 data to create a monthly gridded data product by using global ocean biogeochemical models (GOBMs) as priors and employing machine learning to learn the model-observation misfits. As the climatology of these misfits is the dominant component of the total misfit for all models, the climatology can be used to extend the corrections to the pre-observed period (1959-1982). This allows the LDEO-HPD product to now extend for 66 years (1959 to 2024). In this study we use the LDEO-HPD data product to evaluate the dominant modes of decadal variability of global air-sea CO_2 fluxes and compare the regional contributions to this variability.

2 Methods

2.1 Data and data products

LDEO-HPD interpolates spatiotemporally sparse observations of surface ocean fCO_2 to a global monthly gridded product (Gloege et al., 2022). In this approach, fCO_2 estimates from GOBMs are used as a prior, and then a machine learning algorithm is used to learn the model-observation misfits. With time-varying reanalysis observations that have nearly full global coverage (e.g. sea surface temperature, sea surface salinity, chlorophyll-a, the climatology of mixed layer depths, etc.), the algorithm learns a nonlinear function between observations and the available model-observation misfits of fCO_2. Based on the learned relationship with the full-coverage feature variables, the algorithm can predict full-coverage, time-varying model-observation misfits of fCO_2, which are then added to model fields to create final full-coverage fCO_2 estimates. This process is independently repeated for 10 models used in the 2025 Global Carbon Budget (Friedlingstein et al., 2025; Wright et al., 2021; Aumont et al., 2015; Schwinger et al., 2016; Lacroix et al., 2021; Berthet et al., 2019; Séférian et al., 2019; Gürses et al., 2023; Doney et al., 2009; Tsujino et al., 2024; Sakamoto et al., 2023; Law et al., 2017; Stock et al., 2025). The average of all corrected models is reported as the final fCO_2 estimate in LDEO-HPD. When evaluated against independent data, LDEO-HPD performs marginally better than other data products (Gloege et al., 2022; Bennington et al., 2022).

https://doi.org/10.5194/egusphere-2026-3104
Preprint. Discussion started: 18 June 2026

Surface ocean fCO_2 observations are sufficiently numerous in the 1980s to create data products. Gloege et al. (2021) initially created LDEO-HPD to begin in 1982. Bennington et al. (2022) extended LDEO-HPD to cover also 1959-1981 by applying a climatological correction based on the model-observation misfits since 2000. Because the climatology is the primary contributor to the improvement over the model priors, with the contribution from interannually-varying adjustments being relatively small in comparison, this provides a reasonable correction back in time. Nevertheless, due to the lack of interannual variability in the correction, fCO_2 variability is likely slightly underestimated during the 1959-1981 period (Bennington et al., 2022).

In this study, we use fCO_2 and air-sea flux (FCO_2) estimates from the extended LDEO-HPD data product (Bennington et al., 2022), for 1959 through 2024. Global monthly FCO_2 estimates are made using a bulk parameterization:

$$\mathrm{FCO_2} = k_w \, S_o \, (1 - f_{\mathrm{ice}}) \, (fCO_2 - fCO_{2,\mathrm{atm}}), \tag{1}$$

which parameterizes FCO_2 as a function of the gas-transfer velocity (k_w) calculated from wind speeds, CO_2 solubility (S_o), ice fraction (f_{ice}), the fugacity of CO_2 in the surface ocean (fCO_2) and the water vapor corrected fugacity of CO_2 in the atmosphere ($fCO_{2,\mathrm{atm}}$). A full description of the observational datasets and method used to calculate FCO_2 in LDEO-HPD can be found in Bennington et al. (2022).

To calculate FCO_2 for LDEO-HPD, two monthly gridded reanalysis datasets (1959-2024) from the European Center for Medium Range Weather Forecasts: ERA5 (Hersbach et al., 2023) and ORAS5 (Zuo et al., 2019) are used. For ΔfCO_2 analysis, monthly $fCO_{2,\mathrm{atm}}$ data (1959-2024) are derived from the NOAA Marine Boundary Layer (MBL) xCO_2 reference (1979-2024; Lan et al., 2025), extended back to 1959 using the Mauna Loa trend (Lan et al., 2023).

To study the influence of the atmospheric and oceanic state on FCO_2, we used 10m wind speed data (u_{10}) from ERA5, and SST and mixed layer depth (MLD, defined at a density threshold of 0.03 kg m^{-3}) from ORAS5.

Three climate indices are used for 1959-2024: the multivariate ENSO index (MEI; Wolter and Timlin, 2011; Zhang et al., 2022), the Interdecadal Pacific Oscillation (IPO; Henley et al., 2015) and the Pacific Decadal Oscillation (PDO; Jacobson and Seager, 2025). In this analysis, the extended MEI (Wolter and Timlin, 2011) prior to 1979 is combined with MEI v2 (Zhang et al., 2022) from 1979 onward, bias-correcting MEI v2 to match the extended MEI statistics during their overlap period. The MEI index is representative of the coupled atmosphere-ocean ENSO climate mode of variability, where positive and negative values correspond to El Niño and La Niña events, respectively (Feely et al., 2006). For the IPO, the unfiltered Tripole Index (TPI) from Henley et al. (2015) is used, which captures basin-wide Pacific SST variability on decadal timescales (Power et al., 1999). The PDO index is defined by the leading mode of SST anomalies in the North Pacific, and though its spatial and temporal behavior resemble ENSO, its dominant signal of variability is decadal (Zhang et al., 1997). A positive (negative) PDO is associated with warmer (colder)-than-average SST anomalies in the tropical Pacific (Mantua and Hare, 2002). Here, we use the NOAA Extended Reconstructed SST version 5 (ERSSTv5; Huang et al., 2017)-derived PDO index from Jacobson and Seager (2025), calculated as the leading EOF of North Pacific (20-70°N, 100-250°E) SST anomalies after the global mean is removed. We correlate the MEI, IPO and PDO against the dominant mode of decadal variability of FCO_2 to assess the roles

https://doi.org/10.5194/egusphere-2026-3104
Preprint. Discussion started: 18 June 2026

of climate variability; all three indices are low-pass filtered using the same 3rd-order Butterworth filter with a 7-year cutoff applied to the other variables (see Section 2.3).

2.2 Regional analysis

Based on the basin maps defined by the REgional Carbon Cycle Assessment and Processes (RECCAP) project (Canadell et al., 2011), the global ocean is split into six regions. The six regions are 1) the Atlantic Ocean (southern boundary at 40°S), 2) the Indian Ocean (southern boundary at 40°S), 3) the Southern Ocean (northern boundary at 40°N), and the Pacific Ocean which is further subdivided into 4) the tropical Pacific Ocean (15°N to 15°S region, flanked by the 5) North and 6) South Pacific regions. Limited observations in the Arctic Ocean means that LDEO-HPD estimates here are poorly constrained, and so we leave out the Arctic region in our study.

2.3 Flux and ΔfCO_2 decadal variability

Our analysis focuses on the decadal variability of FCO_2 and the corresponding decadal variability of other atmospheric and ocean variables. To obtain the decadal variability of FCO_2, and other variables, a 3rd-order low-pass Butterworth filter with a 7-year cutoff is applied to linearly detrended and deseasonalized monthly anomalies. Once filtered, 3.5 years are truncated from both ends of the time domain to account for edge effects and so the decadal variability has a shorter period of approximately 1962 to 2021. Unless otherwise stated, data are detrended, deseasonalized and low-pass filtered in order to isolate its decadal variability.

Fluxes are given as rates in units of mol C m^{-2} yr^{-1}. Integrated fluxes (units: PgC yr^{-1}) are presented for the regional time series, allowing for fluxes to be compared between regions that have different areas. Amplitudes of decadal variability of FCO_2 across the different regions are quantified using a measure of one standard deviation (1 s. d.).

For fCO_2 analysis, an additional step is taken prior to detrending. McKinley et al. (2020) show that changes in the growth rate of atmospheric fCO_2 directly imprint onto ocean fCO_2. The trend in ocean fCO_2 is thus nonlinear due to the nonlinear trend in atmospheric fCO_2 (McKinley et al., 2020). The subtraction of $fCO_{2,atm}$ from ocean fCO_2 removes the impact of variability in the $fCO_{2,atm}$ growth rate. Thus, we use the sea-to-air difference in fCO_2 (ΔfCO_2 = fCO_2 - $fCO_{2,atm}$) to investigate ocean sink variability with the imprint of $fCO_{2,atm}$ trend and growth rate variability removed to the first order. As with the FCO_2 analysis, ΔfCO_2 is detrended, deseasonalized and low-pass filtered to isolate its decadal variability.

2.4 Variability analysis

Empirical Orthogonal Function (EOF) analysis is a statistical tool used to identify the modes of variability in data, where each function represents a different mode that is associated with a pattern of variability. The first EOF mode (EOF1) represents the dominant mode of variability in the data. The first principal component (PC1) is its associated time series, which describes the phasing of the spatial patterns in EOF1. Using EOF analysis, we can identify the dominant global pattern of decadal variability of FCO_2 (EOF1-FCO_2) and its corresponding temporal variability (PC1-FCO_2). We assess the significance of EOF

https://doi.org/10.5194/egusphere-2026-3104
Preprint. Discussion started: 18 June 2026

spatial patterns using fractional variance maps. The fractional variance at each gridpoint is a measure of how much of the total variance at a point is explained by the EOF mode. Note that the total variance refers to the total decadal variance, which is not inclusive of interannual, seasonal or sub-seasonal variability.

Next, we compare the contributions of winds and ΔfCO$_2$ to FCO$_2$ variability. FCO$_2$ is parameterized as a function of ΔfCO$_2$ and the gas transfer velocity, which has a quadratic dependence on wind speeds (u$_{10}$), such that FCO$_2$ is proportional to the product of u$_{10}^2$ and ΔfCO$_2$ (Wanninkhof, 2014):

$$FCO_2 \propto (u_{10}^2 \cdot \Delta fCO_2). \tag{2}$$

Using Reynold's decomposition, we separate the mean and the time-varying components of each term as follows:

$$FCO_2 = \overline{FCO_2} + FCO_2', \tag{3}$$

$$\mathrm{u_{10}}^2 = \overline{\mathrm{u_{10}}^2} + \mathrm{u_{10}^2}', \tag{4}$$

$$\Delta\mathrm{fCO_2} = \overline{\Delta\mathrm{fCO_2}} + \Delta\mathrm{fCO_2}', \tag{5}$$

where overbars represent the long-term mean and primes indicate monthly deviations from the long-term mean. Substituting Equations 3-5 into Equation 2, we can write FCO$_2$ variability (FCO$_2'$) as:

$$FCO_2' \propto \overline{u_{10}^2}\, \Delta fCO_2' + \left(u_{10}^2\right)' \overline{\Delta fCO_2} + \mathcal{O}(x^2), \tag{6}$$

where FCO_2', is in units of μatm m^{-2} s^{-2}. $\mathcal{O}(x^2)$ represents the second-order nonlinear term, which is much smaller (Figure 4) than the two linear terms on the right-hand side of Equation 6 and is calculated by subtracting the two linear terms from FCO$_2'$. In Equation 6, the first term on the right is the ΔfCO_2-driven component (i.e. the ΔfCO_2-varying, fixed-wind field); the second term is the u_{10}^2-driven component (i.e. the wind-varying, fixed-ΔfCO_2 field). Long-term means are calculated on raw monthly data, while the monthly ΔfCO_2 deviations are the detrended and deseasonalized monthly anomalies. Monthly u_{10}^2 deviations are calculated on raw monthly data (trend retained). Their product is then computed before low-pass filtering to obtain each components' decadal variability. The decadal roles of u_{10}^2 versus ΔfCO$_2$ in FCO$_2$ decadal variability can be inferred from their relative roles as drivers of FCO_2'.

2.5 Composite

We use composite difference maps of the ocean and atmosphere to illustrate the patterns of change between the periods of positive and negative PC1-FCO$_2$ phase. Composites of raw data are created for the following air-sea flux-related variables: u_{10}^2, SST, and MLD. A composite of detrended and filtered ΔfCO_2 is also created so that changes in the physical system can be attributed to decadal ΔfCO_2 variations around the long-term trend. Composite changes illustrate change from one phase of PC1-FCO$_2$ to the opposite phase. This analysis with six decades of LDEO-HPD allows for re-interpretation of previously-reported fCO_2 trends from the 1990s to 2000s in the context of decadal variability.

https://doi.org/10.5194/egusphere-2026-3104
Preprint. Discussion started: 18 June 2026

3 Results

A multiyear mean map of unprocessed FCO_2 from the LDEO-HPD data product (Figure 1A) shows the well-known features of the natural ocean-atmosphere CO_2 exchange; the largest coherent feature being the CO_2 source in the equatorial Pacific Ocean. The globally-integrated FCO_2 time series (Figure 1B, dark line) shows a long-term increasing ocean sink with large interannual variability, especially in the period between 1980 to 2010, and strong decadal variability. The same is also seen in global ΔfCO_2 (Figure 1C, dark line), which is highly correlated to the FCO_2 (r = 0.98). When the long-term flux trend is removed (Figure 1B, green line), the decadal timescale variability becomes clear. The ocean sink strengthened in the early 1980s, weakened over the 1990s and then strengthened once again from the late 1990s to about 2010. The periods before (1959 through mid 1970s) and after (2010 to 2024) this decadal fluctuation showed sink strength close to the full period mean. The same variability is seen in the decadal variability ΔfCO_2 (Figure 1C, blue line), consistent with ΔfCO_2 being the dominant control on FCO_2.

3.1 Regional contributions to decadal sink variability

A regional breakdown of decadal FCO_2 variability shows which regions have the greatest decadal variability (Figure 2). Comparing the flux rates (units: mol C m^{-2} yr^{-1}), we find that the tropical Pacific and Southern Ocean have the largest flux variability (1σ = 0.11 and 0.13 mol C $m^{-2}yr^{-1}$, respectively). After accounting for the different surface areas of the regions, the tropical Pacific and Southern Ocean still dominate the flux variability (1σ = 0.08 and 0.12 PgC yr^{-1}, respectively).

EOF1 of low-passed FCO_2 (Figure 3A) explains 36% of the total variance in global decadal FCO_2 variability. The dominant features in the EOF1 are the two lobes of high and same-sign variance: one in the tropical Pacific, and the other in the Southern Ocean. While the EOF1 signal over the tropical Pacific has the larger signal, the high variance over the Southern Ocean is extensive and relatively homogeneous. Fractional variances calculated at each point of the global ocean (Figure 3C) shows that most of the variance in the tropical Pacific and Southern Ocean is associated with this EOF pattern.

The associated time series, PC1-FCO_2 (Figure 3B) correlates strongly (r = 0.82, p<0.01; not shown) with the decadal variability of global mean FCO_2 (Figure 1B), emphasizing that this is the dominant pattern of total air-sea CO_2 flux variability. The EOF1 pattern over the tropical Pacific and Southern Ocean can thus be interpreted as an anomalous outgassing signal during positive PC1-FCO_2 periods and an anomalous sink signal during negative PC1-FCO_2 periods. The PC1-FCO_2 is also correlated with the decadal variability of climate modes that are centered around coupled ocean-atmosphere interactions in the Pacific Ocean: the MEI (r = -0.68, p<0.01), the IPO (r=-0.71, p<0.01), and the PDO (r = -0.68, p<0.01; Figure 3B). The negative phases of the indices closely coincide with the positive phases of PC1-FCO_2 and vice versa.

The second mode of variability (EOF2, Figures 3D– 3F) explains 19% of the total variance in global decadal FCO_2 variability. Compared to the first mode, there is less distinct spatial structure in the EOF2 or the fractional variance map.

https://doi.org/10.5194/egusphere-2026-3104
Preprint. Discussion started: 18 June 2026

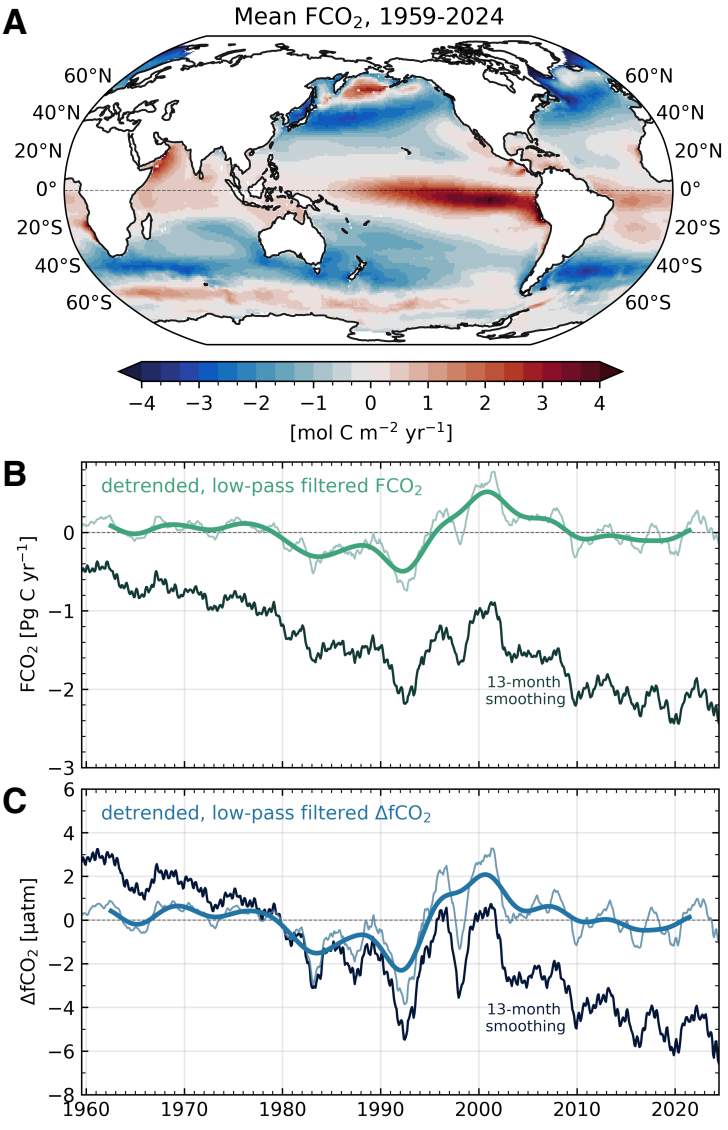

Figure 1. A) Multiyear mean map (1959-2024) of air-sea CO_2 fluxes (FCO_2; units: mol C m^{-2} yr^{-1}) from the extended LDEO-Hybrid Physics Data (LDEO-HPD; Bennington et al., 2022; Gloege et al., 2022) product. Positive fluxes indicate CO_2 outgassing from the ocean to the atmosphere. B) Globally-integrated FCO_2 time series (units: PgC yr^{-1}) with 13-month smoothing (thin, dark line). The detrended time series is shown in green (low-pass filtered, bold line; unfiltered, faint line). C) same as in B) except for ΔfCO_2 (units: μatm) shown in blue; a negative value indicates that atmospheric fCO_2 is greater than oceanic fCO_2.

https://doi.org/10.5194/egusphere-2026-3104
Preprint. Discussion started: 18 June 2026

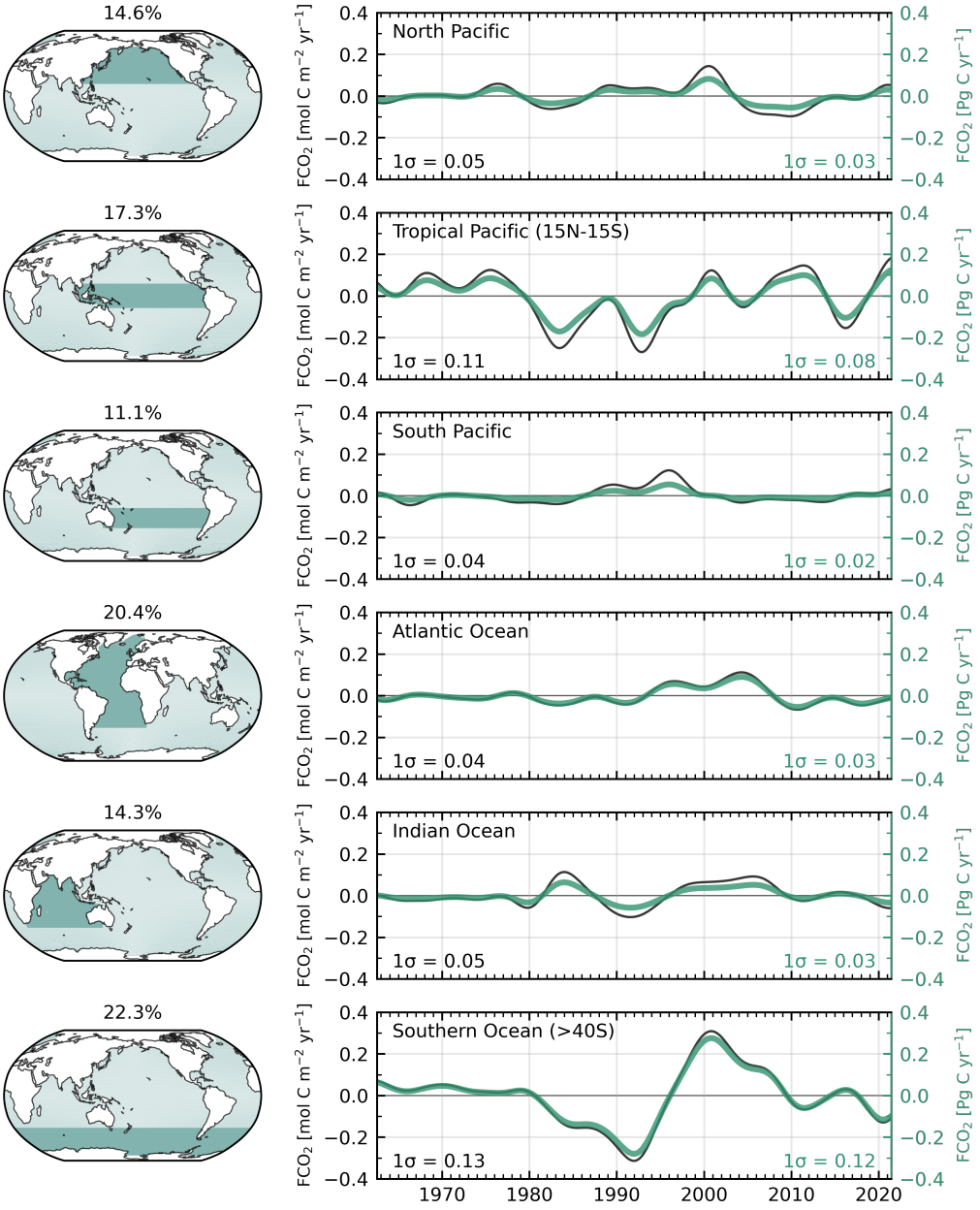

Figure 2. Detrended and low-pass filtered regional air-sea CO_2 fluxes (FCO_2) are presented as both a spatially-averaged flux rate (black line; left axis units: mol C $m^{-2}yr^{-1}$) and a regionally-integrated flux (green line; right axis units: PgC yr^{-1}). Positive fluxes indicate CO_2 outgassing from the ocean to the atmosphere. The standard deviation (1σ, units: mol C $m^{-2}yr^{-1}$ or PgC yr^{-1}) of each time series are denoted by the same color in each panel. The maps represent the different regions (shaded) and its percentage area of the global ocean surface.

https://doi.org/10.5194/egusphere-2026-3104
Preprint. Discussion started: 18 June 2026

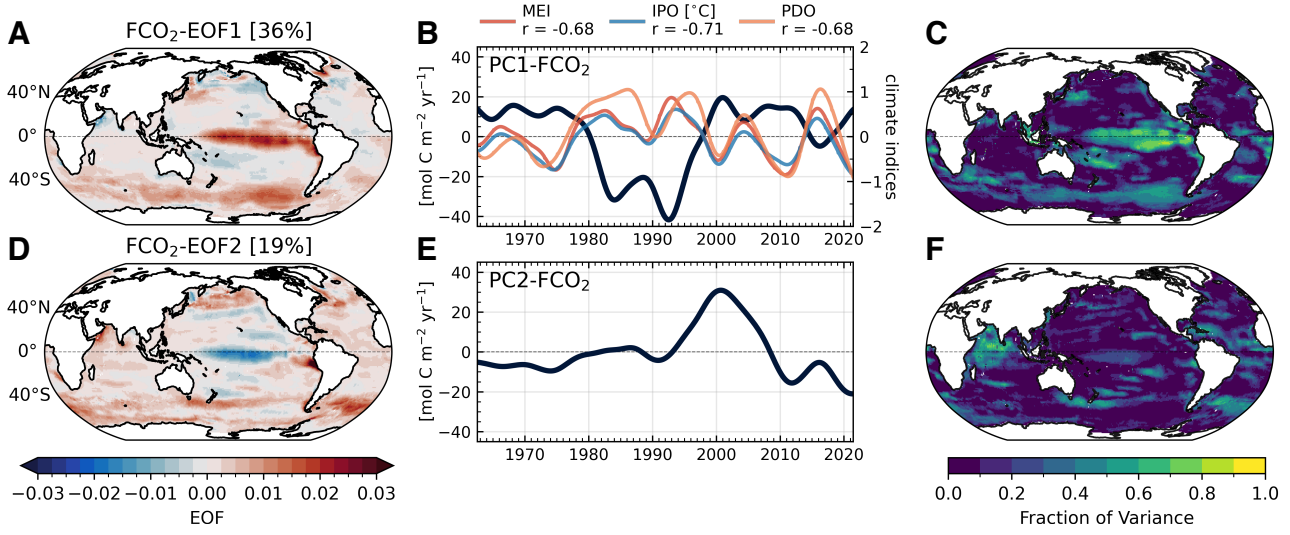

Figure 3. A) First EOF mode (EOF1) of detrended and low-pass filtered FCO_2. The total variance explained by the EOF mode is given as a percentage in the square brackets. B) Time series of the first Principal Component (PC1-FCO_2, black line, units: mol C m^{-2} yr^{-1}; left y-axis) and the time series of three low-pass filtered climate indices (right y-axis): MEI (red), IPO (blue, units: °C) and PDO (orange). Correlation coefficients (r) between climate indices and PC1-FCO_2 are included in the legend. C) Fraction of variance map for the EOF1, where unity implies that the variance explained by the EOF mode at that point explains 100% of the total variance at that point. D-F) The same as in A-C except for the second EOF (EOF2).

3.2 Winds versus ΔfCO_2 as drivers of decadal variability

Figure 4A shows the globally-averaged time series of the total flux-proportionate variability FCO_2' (Equation 6) and its decomposed components of variability: the detrended ΔfCO_2-driven term (blue line), the unprocessed u_{10}^2-driven term (yellow line), and the second-order term (thin black line). Based on the magnitudes of their decadal variability, the ΔfCO_2-driven component (1σ = 57 μatm m^{-2} s^{-2}) overwhelms the modest, typically constructive, effect of the u_{10}^2-driven component (1σ = 15 μatm m^{-2} s^{-2}). Regionally-averaged (as opposed to globally-averaged) plots of the same terms in the tropical Pacific Ocean and the Southern Ocean are similar (Figure 5).

Comparing the EOF1 of the ΔfCO_2-driven component against the EOF1 of the u_{10}^2-driven component (Figures 4B and 4C) we find that the ΔfCO_2-driven component also dominates the spatial mode of variability seen in FCO_2' (Figure 4D) - the EOF1 of the ΔfCO_2-driven component (Figure 4B) and the EOF1 of FCO_2' (Figure 4D) have a high spatial correlation coefficient of r = 0.97. Furthermore, the EOF1 of FCO_2' is highly correlated (r = 0.96) to the EOF1 of FCO_2 (Figure 3A). The associated PC1s show a close correspondence between the ΔfCO_2-driven component and FCO_2'.

https://doi.org/10.5194/egusphere-2026-3104
Preprint. Discussion started: 18 June 2026

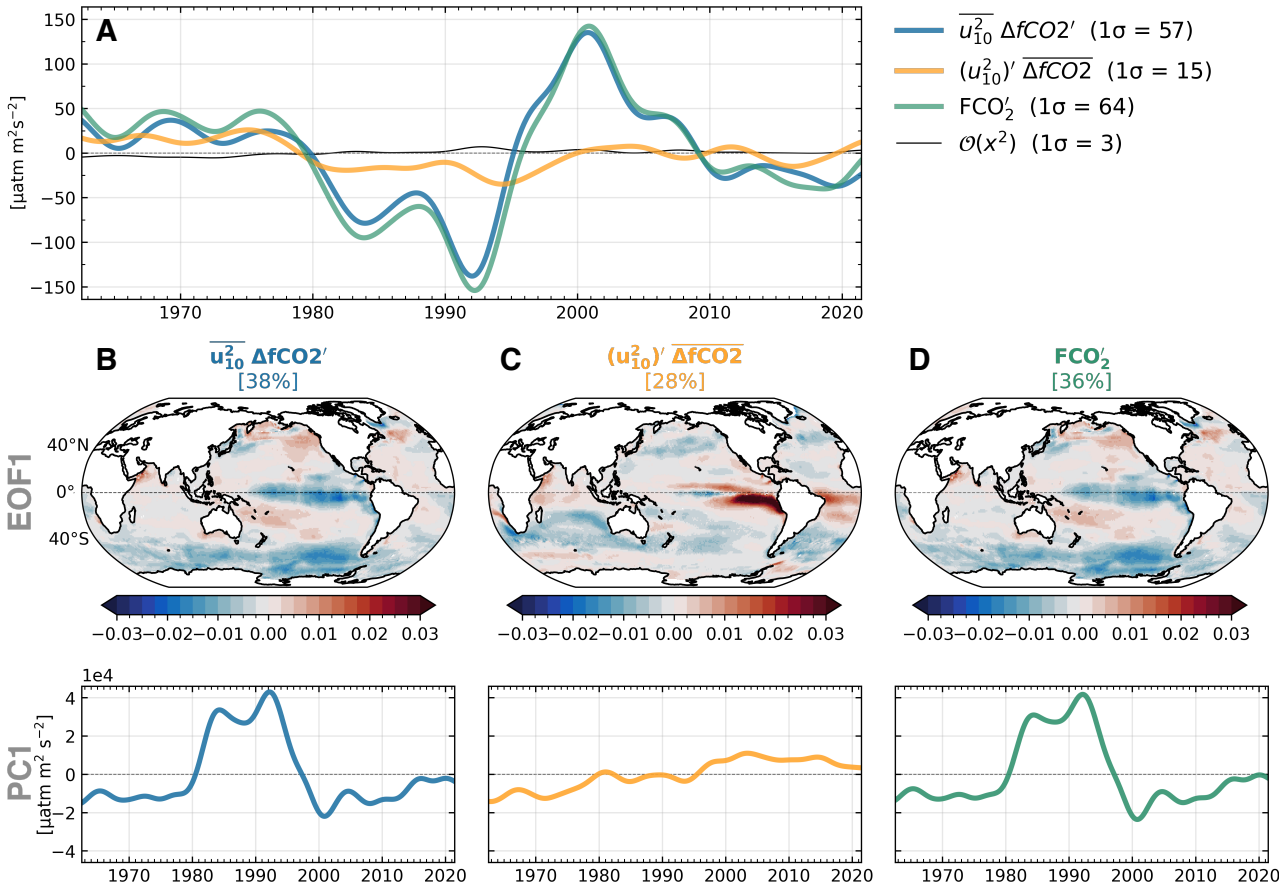

Figure 4. A) Globally-averaged time series of the terms in Equation 6 (units: μatm m^{-2} s^{-2}). Note that the product of ΔfCO$_2$ and wind speeds squared (u$_{10}^2$) are proportional to air-sea CO$_2$ flux, but do not equal flux. The blue line is the time series for the ΔfCO$_2$-driven component of flux-proportionate variability, FCO_2' (green line). The yellow line is the time series for the u_{10}^2-driven component (trend retained) of FCO_2'. The second-order term is the thin black line. FCO_2' is the linear combination of the other three terms. The standard deviation for each term (1σ; units: μatm m^{-2} s^{-2}) is also shown. The first EOF mode (EOF1) and its associated Principal Component (PC1) are shown for the ΔfCO$_2$-driven component (B), the u_{10}^2-driven component (C), and FCO_2' (D). The percentage variance explained by each EOF1 is given in brackets.

https://doi.org/10.5194/egusphere-2026-3104
Preprint. Discussion started: 18 June 2026

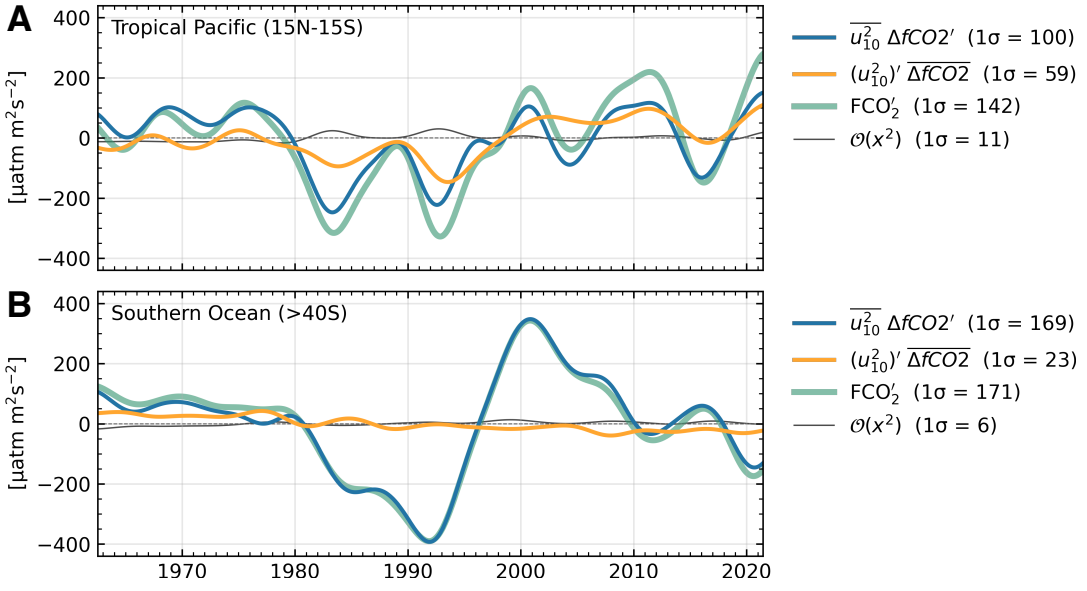

Figure 5. Comparison of u_{10}^2-driven variability against ΔfCO_2-driven variability in the Southern Ocean and tropical Pacific Ocean. The regionally-averaged time series of the terms in Equation 6 (units: μatm m^{-2} s^{-2}) for the Tropical Pacific (A) and the Southern Ocean (B). Note that the product of ΔfCO_2 and wind speeds squared (u_{10}^2) are proportional to air-sea CO_2 flux, but do not equal flux. The blue line is the time series for the ΔfCO_2-driven component of flux-proportionate variability, FCO_2' (green line). The yellow line is the time series for the u_{10}^2-driven component (trend retained) of FCO_2'. The second-order term is the thin black line. FCO_2' is the linear combination of the other three terms. The standard deviation of each term (1σ; units: μatm m^{-2} s^{-2}) is also shown.

3.3 Composites of ΔfCO_2, u_{10}^2, SST and MLD

The PC1-FCO_2 suggests a periodic phenomena with 1.5 cycles of global ocean FCO_2 decadal variability present in the available timeseries. To illustrate the change between the positive and negative phases of this cycle, we composite flux-related variables that have been unprocessed - i.e. no detrending and no filtering (Figure 6B-D), except for the $\Delta fCO_2'$ composite (Figure 6A). The composites represent the positive PC1-FCO_2 phase minus the negative PC1-FCO_2 phase. The negative phase includes the last two decades of the 20$^{\text{th}}$ century (1980 to ∼1998) and a brief period between 2015 and 2018, while the positive phase approximately includes the prior two decades (1959 to 1980), the first decade and a half of the 21$^{\text{st}}$ century (∼1998 to 2015), and from 2018 to 2024. Due to the dominance of the Southern Ocean and the tropical Pacific Ocean in decadal FCO_2 variability (Figures 2, 3 and 4), the discussion of the results below will focus on these two regions.

3.3.1 Tropical Pacific

Figure 6A (right) shows the multiyear mean map of ΔfCO_2 which in the tropical Pacific is positive (i.e. a source of carbon to the atmosphere). Thus, the composite change in $\Delta fCO_2'$ (Figure 6A, left) implies that the tropical Pacific ΔfCO_2 is intensified (and broadened) in the positive phase, strengthening CO_2 outgassing. A positive change in $\Delta fCO_2'$ indicates an increase in

https://doi.org/10.5194/egusphere-2026-3104
Preprint. Discussion started: 18 June 2026

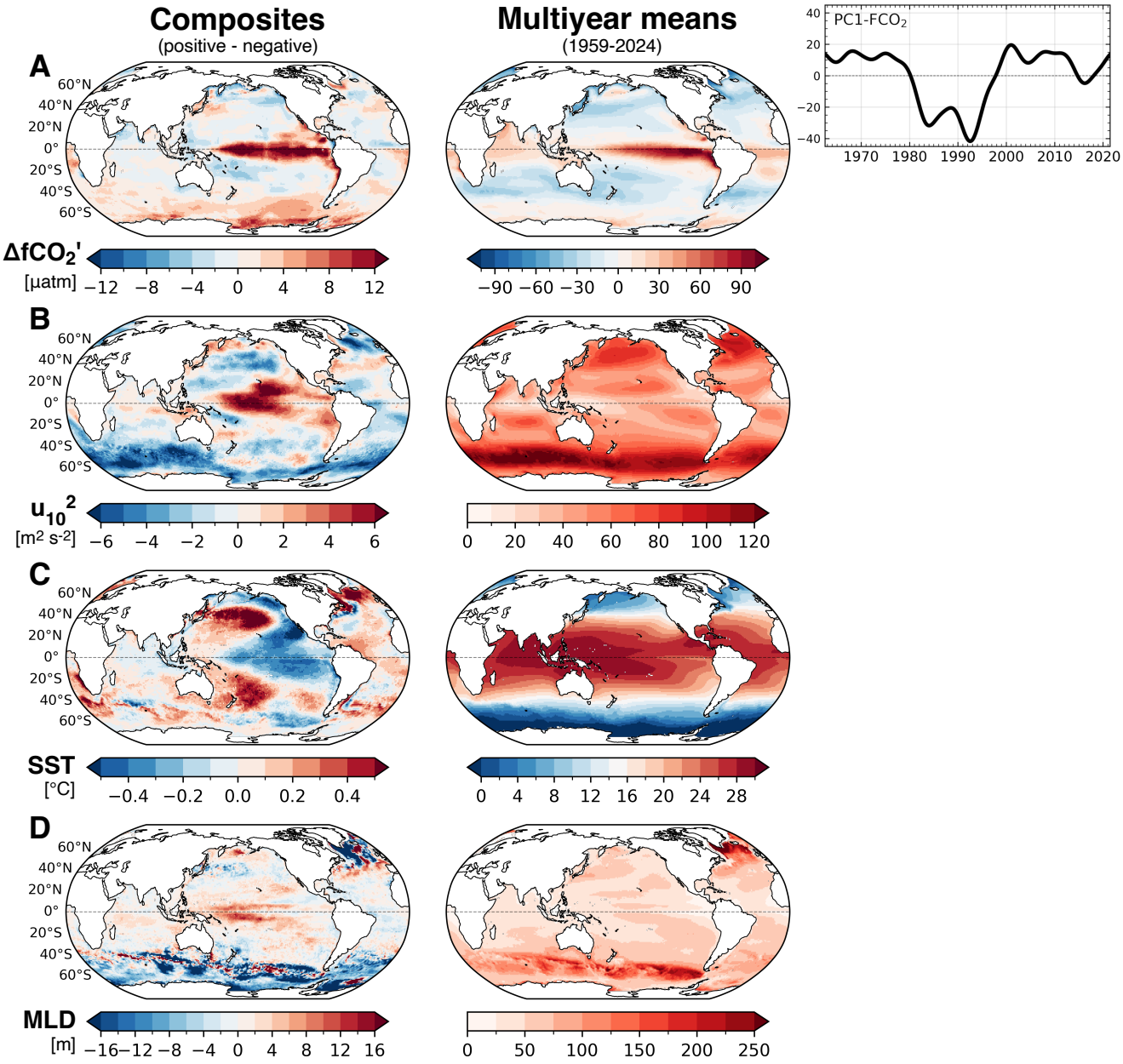

Figure 6. Composite changes in A) $\Delta fCO_2'$ (units: μatm; detrended and filtered), B) u_{10}^2 (units: $m^2 s^{-2}$), C) SST (units: °C), and D) MLD (units: m) are evaluated over the full period of PC1-FCO_2 (1962-2021; inset is from Figure 3B). The composite difference is defined as positive minus negative phases of the PC1-FCO_2. Multiyear mean maps (1959-2024) of each variable are shown to the right of their composites to provide context for interpretation; the multiyear mean map for $\Delta fCO_2'$ is calculated with unprocessed ΔfCO_2. Sign conventions: positive ΔfCO_2 means that oceanic fCO_2 is greater than atmospheric fCO_2; MLD is positive downwards, such that positive composite values indicate MLD deepening.

https://doi.org/10.5194/egusphere-2026-3104
Preprint. Discussion started: 18 June 2026

ocean fCO_2 since the data are detrended. A strengthened CO_2 source in the tropical Pacific coincided with an increase in u_{10}^2 (higher wind speeds, Figure 6B), a decrease in SSTs (cooler surface ocean, Figure 6C) and a basin-wide increase in MLDs across the tropical Pacific (Figure 6D), except for the shoaling MLDs over the eastern equatorial Pacific and off the coast of Peru. These changes are consistent with the La Niña phase that is dominant in the positive composite period.

3.3.2 Southern Ocean

In the Southern Ocean, the multiyear mean of ΔfCO_2 is negative ($\overline{\Delta fCO_2}$ = -17.1 μatm; i.e. a sink) and the composite change in $\Delta fCO_2'$ is positive over most of the Southern Ocean (Figure 6A) indicating that the Southern Ocean sink weakens with the positive phase. The weaker Southern Ocean sink coincided with an overall decrease in u_{10}^2 (weaker wind speeds, Figure 6B) except in parts of the South Pacific, and a general (consistent) decrease in MLDs over the region (mixed layer shoaling, Figure 6D; $\overline{\Delta MLD}$ = -5.3 m over the Southern Ocean). For the SST composite, (Figure 6C), there is large SST cooling in the Pacific sector of the Southern Ocean where u_{10}^2 strengthened and warming south of Australia where wind speeds strengthened. See Figure A1 for Southern Ocean polar stereographic projections.

4 Discussion

4.1 Ocean sink variability in LDEO-HPD

The temporal extension of LDEO-HPD (Bennington et al., 2022) back to 1959 offers more than six decades of FCO_2 and fCO_2 estimates, a temporal increase of about 50% compared to most other products (Fay et al., 2021; Gruber et al., 2023). Decadal FCO_2 variability in LDEO-HPD (Figure 1B) is consistent with previous studies of global sink variability since the 1980s, specifically the weakened sink in the 1990s and the recovery of the sink in the 2000s (Fay et al., 2014; Landschützer et al., 2016; DeVries et al., 2019; Hauck et al., 2020; McKinley et al., 2020; Gruber et al., 2023). LDEO-HPD's extended temporal coverage indicates that these previously-reported changes are a segment of multi-decadal variability, identified here with EOF analysis (Figure 3B).

LDEO-HPD indicates that throughout the 1960s and 1970s the ocean sink was weaker than the 6 decade average and then around 1980, the sink strengthened. The previously-reported weakening of the sink in the late 1990s can be viewed as a readjustment of the sink state to that of the 1960s and 1970s. The extension of time coverage by LDEO-HPD to 1.5 cycles of this variability adds important context for many previous trend analyses that have been more limited in temporal extent, starting from the 1980s or 1990s (Fay et al., 2014; Landschützer et al., 2016; DeVries et al., 2019; McKinley et al., 2020; Gruber et al., 2023). These variations in the sink are composed of like-sign variations in the tropical Pacific and Southern Ocean with both having increased outgassing in the 1960s and 1970s.

As LDEO-HPD is a hybrid reconstruction, incorporating information from 10 hindcast ocean models and Surface Ocean CO_2 Atlas (SOCAT; Bakker et al., 2016) fCO_2 data, it is useful to ask how much of the decadal variability in this data product is due to the models vs. the data. We explore this topic in the Appendix, with major findings being that the data drives significant

https://doi.org/10.5194/egusphere-2026-3104
Preprint. Discussion started: 18 June 2026

mean-state adjustments in all regions. The models fully determine the decadal variability of the LDEO-HPD product prior to 1982, as expected. Beyond 1982, the observations have the greatest impact on the variability in the Southern and Indian Oceans, with impacts increasing as more data become available after 2000.

The sink in the 1960s and 1970s may be sensitive to the construction methods of LDEO-HPD which differs between 1959-1981 and 1982-present (Bennington et al., 2022). For the later period, Bennington et al. (2022) used machine learning to determine an interannually-varying misfit, and then applied these full-field estimates to adjust each modeled fCO_2 toward the data. Due to the lack of ocean carbon observations prior to 1982, a climatological adjustment based on the model-data misfits of 2000-2024 is applied prior to 1982; justified by the climatology being the far-dominant component of the misfit. This correction does not vary significantly if a different subset of years is used to create the climatological adjustment.

The GOBMs are forced with reanalyses that suffer from a sparsity of meteorological observations in their earlier decades, which may also lead to damped variability (Bromwich and Fogt, 2004). Damped variability prior to 1982 is suggested by the components of FCO_2' (Figure 4B-D): the ΔfCO_2-driven PC1 appears to be more variable in the 2000s compared to the years prior to 1982. Thus, we have several reasons to suspect that the magnitude of the sink in the 1960s and 1970s may actually have been weaker during that period (Figure 1B). If this were the case, the sink strengthening around 1980 may have been more pronounced.

It is also possible that the amplitude of decadal variability may be overestimated by LDEO and other fCO_2 data products. Experiments with ocean models as testbeds to explore reconstruction skill have demonstrated that undersampling of fCO_2 in the Southern Ocean contributes to overestimation of FCO_2 decadal variability (Gloege et al., 2021; Hauck et al., 2023). The magnitude of this overestimation varies with data product (Fay et al., 2025).

4.2 Drivers of regional decadal variability

This analysis indicates that decadal changes in ΔfCO_2 and FCO_2 are connected to decadal variations in the physical Pacific ocean-atmosphere system with expression from pole to pole (Di Lorenzo et al., 2023). The tropical Pacific Ocean and the Southern Ocean are the dominant, same-sign, sources of this decadal variability (Figure 2), consistent with previous shorter-term analyses (Gruber et al., 2023) and a prior study of natural variability in Earth System Models (Resplandy et al., 2015). Correlations of the timeseries of FCO_2 reveal that the tropical Pacific and Southern Ocean are the most correlated of all regions (Figure 2; $r = 0.60$, $p<0.05$). The EOF1 of FCO_2 also reveals coherent variability across these two regions (Figure 3A).

The timeseries of the dominant mode of air-sea CO_2 flux variability (PC1-FCO_2) is well correlated with the MEI, IPO and PDO indices (Figure 3B). Negative index phases coincide with the positive phases of PC1-FCO_2 (1959 to 1980; 1998-2015; 2018-2024) and positive index phases roughly coincide with the negative phase of PC1-FCO_2 (1980-1998; 2015-2018). The changes shown in the composites (Figure 6) are centered around PC1-FCO_2 phase shifts that occur at approximately the same times as when the climate indices shift between positive and negative phases. Thus, the decadal FCO_2 variability appears related to the decadal variability of these climate indices and phenomena. The smoothed MEI, IPO and PDO indices are strongly correlated with each other ($r > 0.88$, not shown), which is consistent with the understanding that ENSO and the

https://doi.org/10.5194/egusphere-2026-3104
Preprint. Discussion started: 18 June 2026

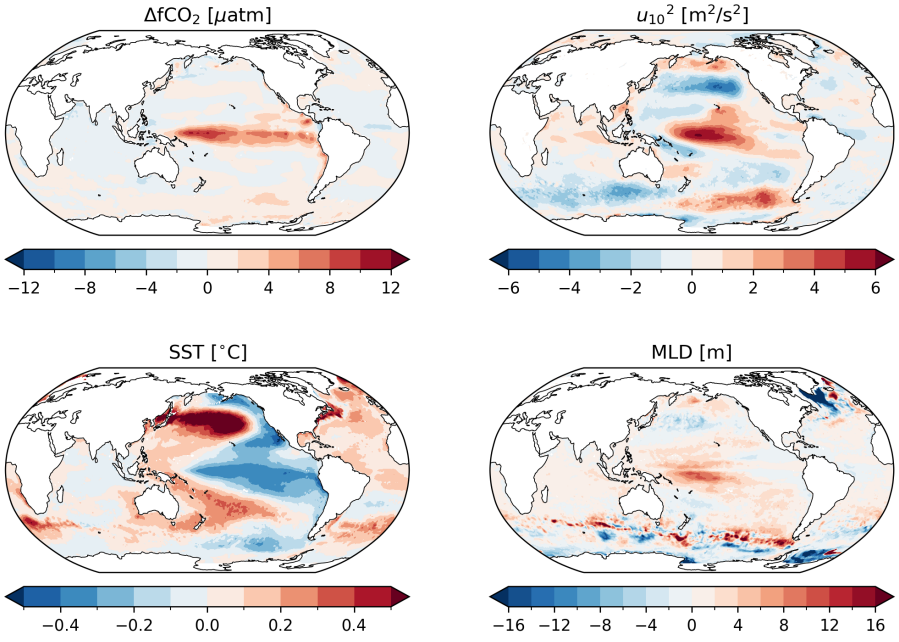

Figure 7. PDO-attributable composites (1962-2021) of $\Delta fCO_2'$, u_{10}^2, SST and MLD. For each variable, values are regressed onto the PDO index, and the regression-predicted values are composited over the same positive and negative PC1-FCO_2 years used in the total composite in Figure 6. These composites represent the component of variability attributable to PDO.

PDO/IPO are strongly linked in a pan-Pacific mode of climate variability that connects across space and timescales (Deser et al., 2012b; Newman et al., 2016; Landschützer et al., 2019; Heidemann et al., 2024; Jacobson and Seager, 2025).

To examine this further, in Figure 7 we show the PDO-attributable change in $\Delta fCO_2'$, u_{10}^2, SST and MLD for the same years that go into the PC1-FCO_2-based composite (Jacobson and Seager, 2025). This is done by first computing regressions of these fields on the PDO index (Figure 3) and then using the index values of years to compute the PC1-FCO_2-based composite. Comparison of Figure 7 to Figure 6 (left column) makes clear that the change in PDO state is contributing considerably to the total change in fCO_2 and physical quantities over these time intervals. Positive (negative) PDO phases are associated with warmer (colder)-than-average SSTs in the tropical Pacific (Mantua and Hare, 2002) and opposite sign SST anomalies in the extratropical Pacific Ocean, a pattern that is also seen in the PC1-FCO_2-based composite (Figure 6C). Positive (negative) PDO phases are also associated with weaker (stronger) wind speeds in the South Pacific west of the tip of South America and opposite sign anomalies in the Indian Ocean sector of the Southern Ocean. The PC1-FCO_2-based composite of u_{10}^2 (Figure 6B) indicates a strengthening from the 20th into the 21st centuries of surface wind speeds in the Southern Ocean which is therefore consistent with the PDO shift in the late 1990s (Garreaud and Battisti, 1999; Pezza et al., 2007).

Kang et al. (2024, 2025) have noted the cooling of the eastern tropical Pacific over this time interval has driven an increase in South Pacific storminess and westerlies, consistent with our results. However, we also note that u_{10}^2 is not detrended for the

https://doi.org/10.5194/egusphere-2026-3104
Preprint. Discussion started: 18 June 2026

composite analysis and so the influence of rising greenhouse gases and the recovery of stratospheric ozone towards the 2000s, which can strengthen the Southern Hemisphere jet stream, could also help explain the strengthened surface wind speeds seen in the composite (Sexton, 2001; Arblaster and Meehl, 2006; Gerber and Son, 2014). Formal detection and attribution work is required to separate the influences of greenhouse gases and ozone from climate variability on surface wind speeds. Li and England (2020) find that variability of winter mixed layers in the Southern Ocean is controlled by teleconnections originating from the Pacific region through ENSO and that multidecadal variability in mixed layer properties are likely to have been influenced by shifts in the Interdecadal Pacific Oscillation (or the PDO).

In the tropical Pacific, the dominant signal of spatial variability is akin to the EOF pattern for ENSO-driven flux interannual variability (McKinley et al., 2004; Wong et al., 2022). The composite patterns over the tropical Pacific (Figure 6) can also be explained by decadal variations in the dominant state, with more La Niña-like conditions in the 1960s and 1970s, more El Niño-like conditions in the 1980s and 1990s, and then more La Niña-like conditions again after 2000. With a more La Niña-like state of the tropical Pacific, stronger easterly trade winds induce stronger upwelling in the eastern tropical Pacific, which both cools the surface ocean and intensifies CO_2 outgassing (Bjerknes, 1966; McKinley et al., 2004; Wong et al., 2022).

Composite patterns in the Southern Ocean (Figures 6 and A1) show that over most of the region, other than some parts of the South Pacific sector, as wind speeds weakened from the late 20^{th} to early 21^{st} century, the MLDs (consistently) shoaled (Sallée et al., 2010). MLD shoaling would be expected to reduce the amount of DIC in the mixed layer, due to the positive downwards DIC gradient in the ocean (Levy et al., 2013; Yang et al., 2021). This would make ΔfCO_2 more negative and strengthen the Southern Ocean sink. Yet, we find spatial coherence across the composite changes over the Southern Ocean which indicate that a regional reduction in MLDs corresponds to a regional positive growth in ΔfCO_2 and a weakened Southern Ocean sink.

An alternative explanation may be that reductions in mixed layer depths created smaller mixed layer volumes and more accumulation of carbon fluxed in from the atmosphere (Fassbender et al., 2017). The complication is that reduced mixing should also reduce the supply of nutrients to the surface layer, and in turn, reduce removal of carbon through biological production of organic carbon and its export to depth. Multiple lines of evidence suggest the biological pump plays a significant role in the variability of the Southern Ocean carbon sink. A constrained global ocean model with biogeochemistry (ECCO-Darwin, Carroll et al. (2022)) finds net biological removal of DIC from the upper 100m of the Southern Ocean, while net diffusive processes, air-sea CO_2 fluxes and net advection drive DIC gain that opposes the significant biological loss term. Huang et al. (2023) also find that biology has an important role in sustaining the Southern Ocean carbon sink. A recent observational study investigated six seasonal cycles of variability using an observations-based Southern Ocean mixed layer DIC budget (Sauvé et al., 2023) and found that biological activity and advection (dominated by Ekman transport) dominated seasonal variations in mixed layer DIC concentrations. The lack of observed products to constrain decadal timescale changes in biological productivity since the 1960s is an impediment to further exploration of this potential mechanism.

In addition to better understanding biological factors, further research is needed to determine how changes in wind stress and surface buoyancy fluxes drive mixed layer depth variability, and how in turn, these are related to modes of climate variability, such as the MEI (Wang et al., 2022), the IPO, the PDO, and the Southern Annular Mode (see Sallée et al., 2010). Goyal et al. (2021) assess ERA5 reanalysis trends (from 1979 to 2019) in southern hemisphere surface westerlies and find that variations in

https://doi.org/10.5194/egusphere-2026-3104
Preprint. Discussion started: 18 June 2026

the position and strength of the westerlies are dominated by natural interannual to decadal scale climate variability. Kang et al. (2024, 2025) also note that the change in winds over the South Pacific were driven by the change in equatorial Pacific SSTs. While it is reasonably known how modes of climate variability influence tropospheric circulation, it is less well known how they influence surface wind speed - with its connection to storminess - and why. Further, the decadal timescale difference in fCO_2 and FCO_2, between the early 21^{st} and late 20^{th} century, will contain some component of responses to time-varying changes in ozone and CO_2 that are not removed by linear detrending. To further complicate matters, there is an active and unresolved debate about whether tropical Pacific trends over the last few decades analyzed here are natural variability, radiatively-forced, or some combination (e.g. Jiang et al., 2024). Other sources of decadal variations to consider include the impacts of volcanic eruptions on the carbon cycle and on ENSO conditions themselves (Eddebbar et al., 2019; McKinley et al., 2020; Fay et al., 2023). Future work needs to disentangle the roles of internal variability, external forcing and ENSO-volcano effects to better understand the decadal variability of the ocean carbon system.

5 Conclusions

The LDEO-HPD product offers a model-data hybrid assessment of 66 years of full-coverage observation-based estimates of ocean fCO_2 and FCO_2. This allows for study of decadal variations in the ocean carbon cycle and their associations with decadal variations of climate. The long timeseries is sufficient to reveal more than a full cycle of decadal variability, with EOF analysis confirming that the decadal variability is a dominant signal. The tropical Pacific Ocean and Southern Ocean are the main contributors to the global decadal variability of FCO_2. The dominant EOF mode of FCO_2 decadal variability is synchronous across these two regions, and is strongly correlated with the modes of variability common to both regions, such as the MEI, IPO and PDO.

Composite changes in physical variables (SST, u_{10}^2 and MLD) reveal patterns of change potentially connected to FCO_2 decadal variability. Decadal changes over the tropical Pacific are consistent with decadal shifts in the PDO or IPO. In the Pacific sector of the Southern Ocean, we do not find a clear mechanistic driver for a weakened carbon sink in the early 21st century, potentially due to biases in the data product or missing information about changes in biological processes.

To better constrain FCO_2 decadal variability and its mechanisms, data products need to be continually updated and improved. Critical for reducing uncertainty will be sustaining existing sampling programs and expanding sampling in data-poor regions (Heimdal et al., 2024; Heimdal and McKinley, 2024; Dong et al., 2024). Understanding decadal variations in the global ocean carbon sink and their connection to decadal timescale climate variation, is an essential component of accurate diagnosis and prediction of the evolving global carbon cycle and climate change.

https://doi.org/10.5194/egusphere-2026-3104
Preprint. Discussion started: 18 June 2026

Appendix A

To understand how much of the variability in LDEO-HPD is driven by the underlying 10 GOBMs (Section 2.1) as opposed to the SOCAT data (Bakker et al., 2016) to which it is corrected, we compare the ΔfCO_2 timeseries of the individual GOBMs, the GOBM mean, and LDEO-HPD (Figure A2). The data-driven correction significantly alters the mean state of most models. Smoothed anomalies of the global timeseries (bottom) show that all pre-1982 variability on timescales longer than 13-months is due to the models, as expected. After 1982, the data adjustments increasingly modify the variability.

The regional decomposition of the individual GOBMs, the GOBM mean, and LDEO-HPD (Figure A3) has qualitatively different impacts on the interannual variability in different regions. The data have limited impact on the phasing of interannual variability in the tropical Pacific, but do modify the amplitude of this variability here. This indicates that, for the majority of GOBMs, the use of reanalysis winds to force the ocean models leads to successful representation of the phasing of ENSO and its impacts on fCO_2. The data do modestly amplify the magnitude of these impacts over the GOBM mean. The data drives the largest regional changes to interannual to decadal variability in the Southern and Indian Oceans.

Correlations over different time periods (Table A1) again demonstrate that prior to 1982 (second column), the 13-month smoothed variability of the GOBM mean fully explains LDEO-HPD variability, with all correlations being 0.99 or 1.0. However, for 2000-2024, when SOCAT data have the greatest density, the GOBM mean is poorly correlated to LDEO-HPD in the Southern and Indian Oceans, as well as in the Atlantic. In these basins, the data is the dominant cause of the 13-month smoothed variability. Correlations for 1982-1998 are intermediate, consistent with a more balanced influence of the models and the SOCAT data. As noted above, the data do not substantially change the phasing of Tropical Pacific variability, and thus correlations are 0.88 or higher for all timeframes here.

This brief analysis is a first look at the relative influence of the GOBMs and the SOCAT data on the decadal variability of the LDEO-HPD product. We find that the pattern of coherent tropical Pacific / Southern Ocean variability revealed by LDEO-HPD is the combined result of an ensemble of GOBMs that collectively can capture the phasing and most of the amplitude of tropical Pacific decadal variability, but that do not, as an ensemble, capture Southern Ocean decadal variability. Southern Ocean decadal variability is significantly modified when the SOCAT data correction is applied, leading to the coherent features discussed in the main text. Future analysis should evaluate the signals in the different models when they are adjusted, and further quantify how the models and the data-based adjustments work together to reconstruct the decadal variability of the ocean carbon sink.

https://doi.org/10.5194/egusphere-2026-3104
Preprint. Discussion started: 18 June 2026

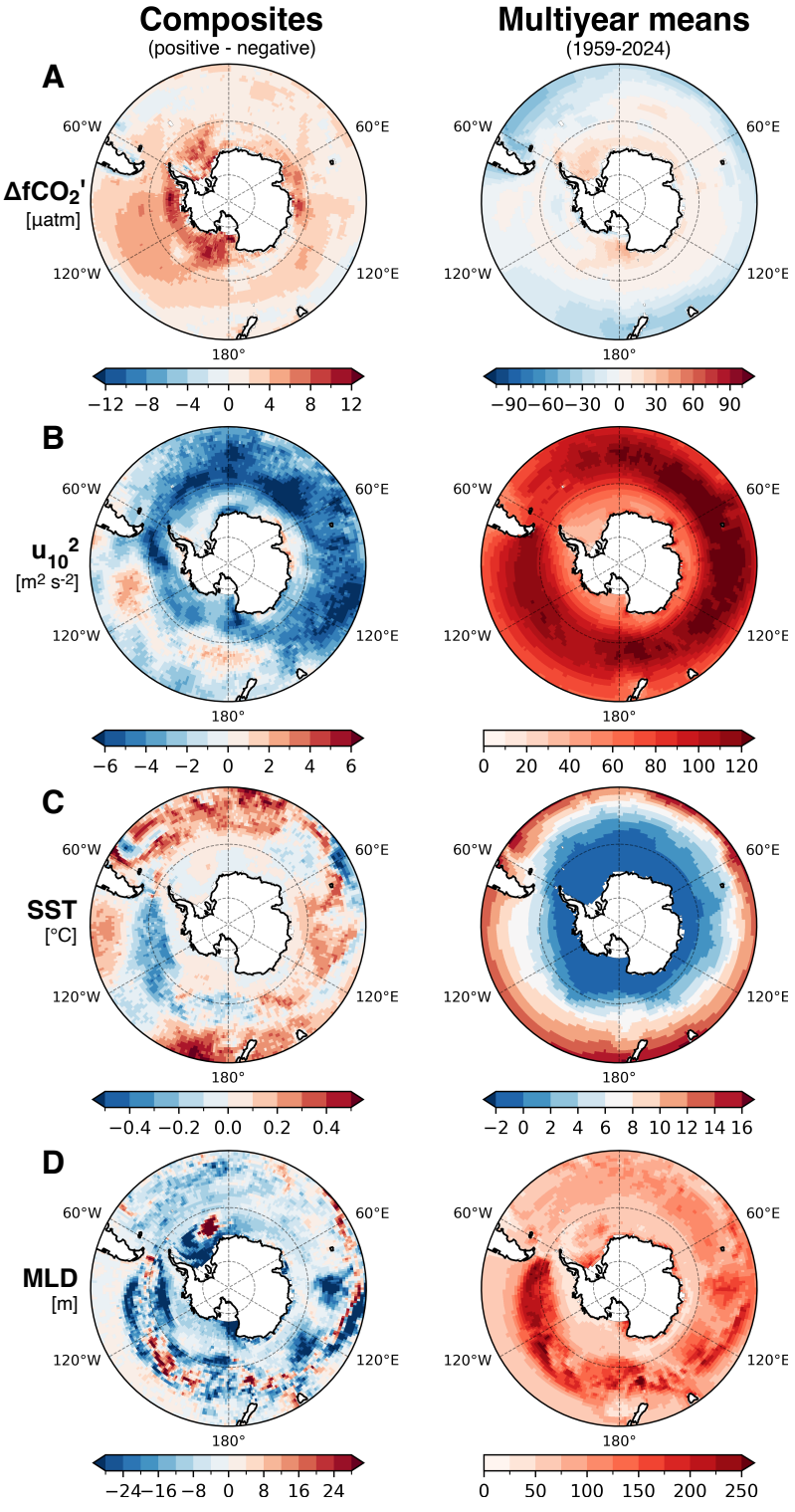

Figure A1. Southern Ocean view (polar stereographic, >40°S) of Figure 6.

https://doi.org/10.5194/egusphere-2026-3104
Preprint. Discussion started: 18 June 2026

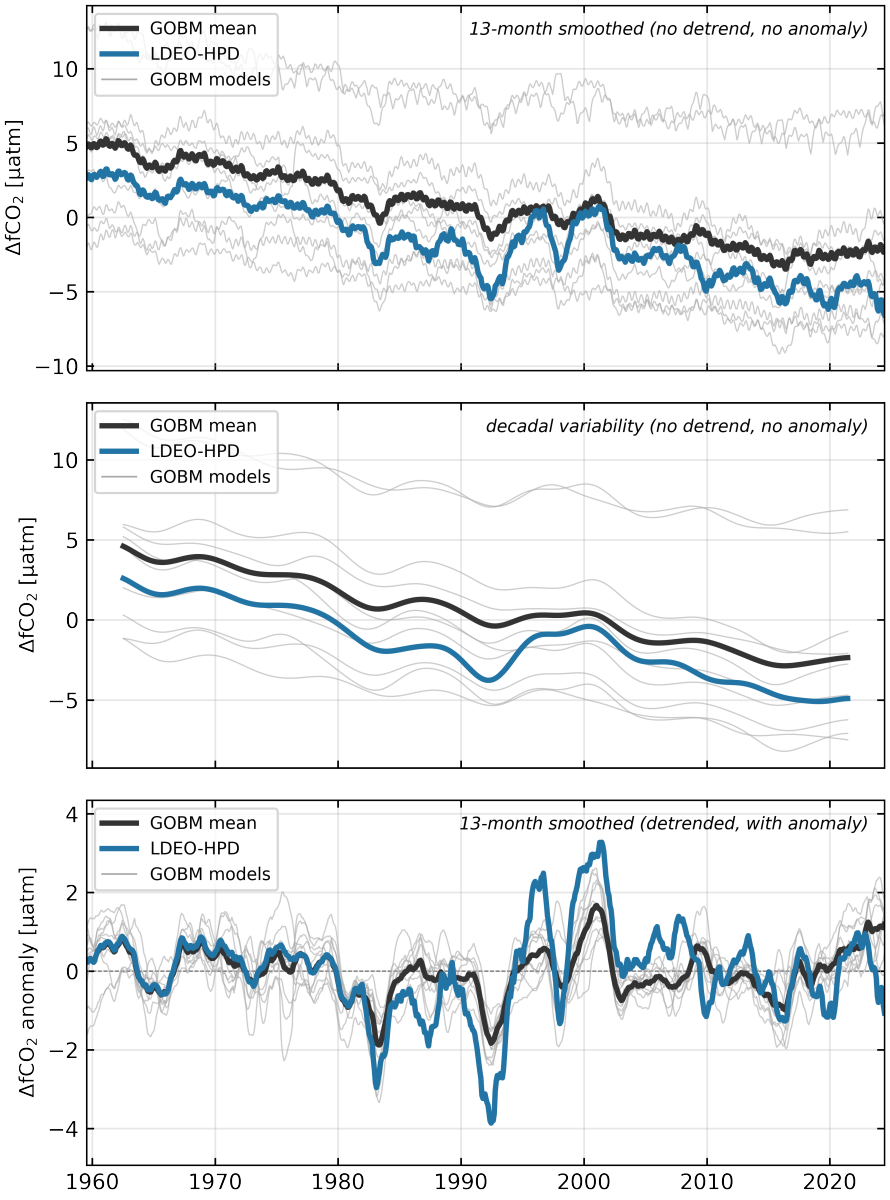

Figure A2. Global ocean ΔfCO_2 1959-2024 time series comparing LDEO-HPD (blue) against 10 Global Ocean Biogeochemical Models (GOBMs) from the Global Carbon Budget 2025 (gray lines: individual models; black line: multi-model mean). Top panel: 13-month smoothed ΔfCO_2 (no detrending). Middle panel: lowpass-filtered decadal variability of ΔfCO_2 (no detrending). Bottom panel: 13-month smoothed ΔfCO_2 anomaly after linear detrending. All time series are area-weighted global means. The top two panels retain the long-term trend, while the bottom panel isolates interannual variability.

https://doi.org/10.5194/egusphere-2026-3104
Preprint. Discussion started: 18 June 2026

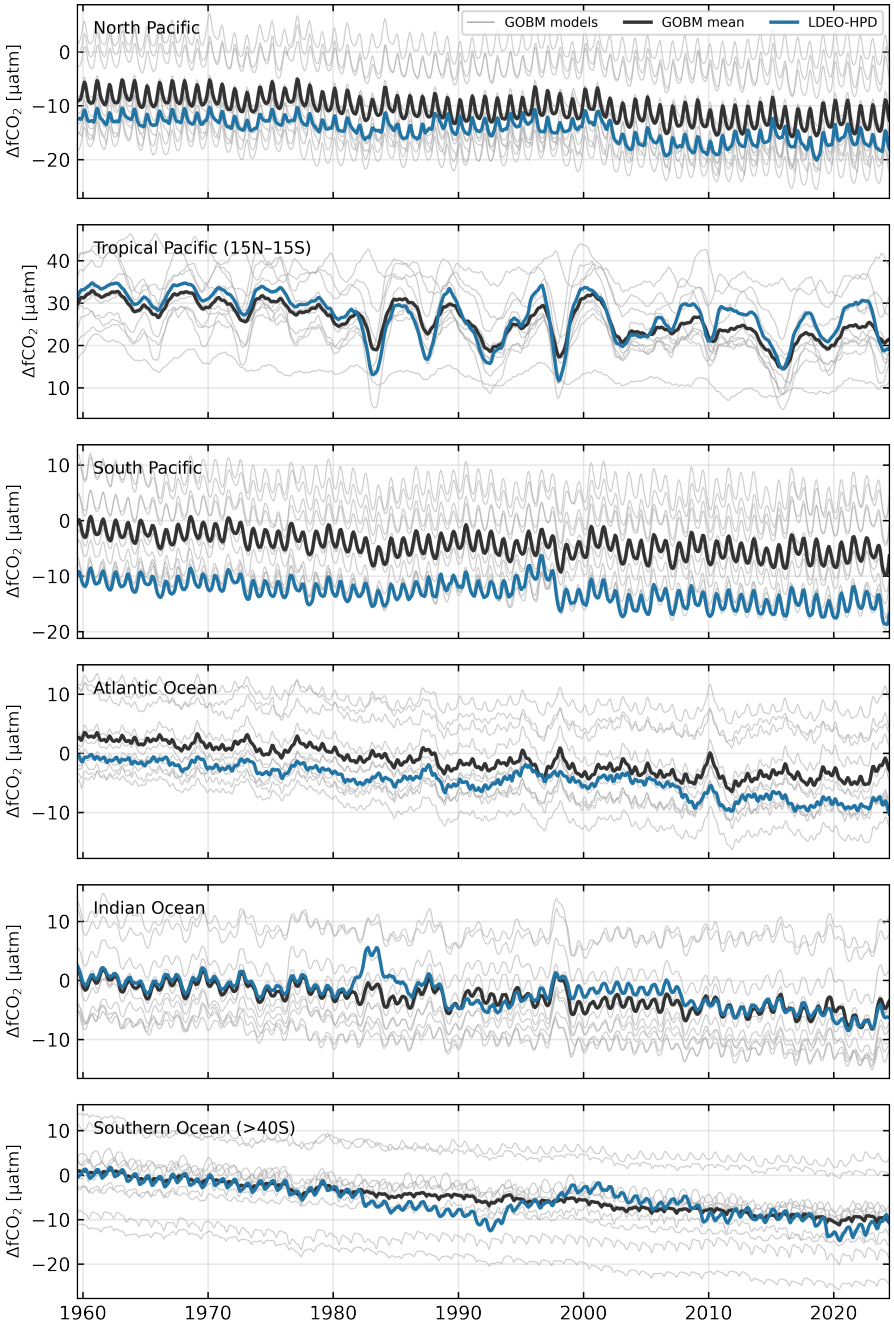

Figure A3. Regional ΔfCO_2 1959-2024 time series comparing LDEO-HPD (blue) with 10 GOBMs from the Global Carbon Budget 2025 (gray lines: individual models; black line: multi-model mean). Panels show, from top to bottom: North Pacific, Tropical Pacific (15°N–15°S), South Pacific, Atlantic Ocean, Indian Ocean, and Southern Ocean (>40°S). All time series are area-weighted regional means smoothed with a 13-month running mean. No detrending is applied.

https://doi.org/10.5194/egusphere-2026-3104
Preprint. Discussion started: 18 June 2026

Table A1. Detrended correlation coefficients between area-weighted, 13-month smoothed, detrended ΔfCO_2 time series from the GOBM multi-model mean and LDEO-HPD, computed for each region and the global domain over five time periods. The linear trend has been removed prior to calculating the correlation coefficients. For the sub-period correlations (1959-1980, 1982-1998, and 2000-2024), a 2-year gap is used between adjacent windows to avoid confounding effects from the 13-month smoothing.

Region	1959–2024	1959–1980	1982–1998	1982–2024	2000–2024
North Pacific	0.71	0.98	0.63	0.72	0.79
Tropical Pacific (15°N–15°S)	0.89	0.99	0.92	0.89	0.88
South Pacific	0.63	1.00	0.80	0.60	0.91
Atlantic Ocean	0.50	0.99	0.70	0.46	0.35
Indian Ocean	0.48	0.99	0.43	0.40	0.37
Southern Ocean (>40°S)	0.41	1.00	0.64	0.39	-0.01
Global	**0.75**	**0.98**	**0.84**	**0.73**	**0.55**

https://doi.org/10.5194/egusphere-2026-3104
Preprint. Discussion started: 18 June 2026

. **Data Availability:** No new data were generated for this study. The LDEO-HPD product and its code can be accessed from https://oceancarbon.ldeo.columbia.edu.

. **Author Contribution:** SCKW, GAM and RS conceived of the project, and SCKW conducted the analysis and drafted the manuscript. Other authors contributed datasets, code and revised the manuscript.

. **Competing Interests:** The authors have no competing interests to declare.

. **Acknowledgements:** We acknowledge support from the National Science Foundation through the LEAP Science Technology Center (AGS-2019625) and the Graduate School of Columbia University. TJ acknowledges the NERC Frontiers project (NE/V011103/1). The Surface Ocean CO_2 Atlas (SOCAT) is an international effort, endorsed by the SCOR Infrastructural Project International Ocean Carbon Coordination Project (IOCCP) and the Surface Ocean Lower-Atmosphere Study (SOLAS), to deliver a uniform, quality-controlled surface ocean CO_2 database. The many researchers and funding agencies responsible for the collection of data and quality control are thanked for their contributions to SOCAT. RS was supported by NSF awards OCE-2219829 and OCE-2445981. TI acknowledges the European Union's Horizon Europe research and innovation program under grant agreement no. 101137682 (AI4PEX).

https://doi.org/10.5194/egusphere-2026-3104
Preprint. Discussion started: 18 June 2026

References

Copernicus Climate Change Service, Climate Data Store, (2021). ORAS5 global ocean reanalysis monthly data from 1958 to present. [Dataset] Copernicus Climate Change Service (C3S) Climate Data Store (CDS)., https://doi.org/10.24381/cds.67e8eeb7.

Arblaster, J. M. and Meehl, G. A.: Contributions of External Forcings to Southern Annular Mode Trends, Journal of Climate, 19, 2896 – 2905, https://doi.org/10.1175/JCLI3774.1, https://journals.ametsoc.org/view/journals/clim/19/12/jcli3774.1.xml, 2006.

Aumont, O., Ethé, C., Tagliabue, A., Bopp, L., and Gehlen, M.: PISCES-v2: an ocean biogeochemical model for carbon and ecosystem studies, Geoscientific Model Development, 8, 2465–2513, https://doi.org/10.5194/gmd-8-2465-2015, 2015.

Bakker, D. C. E., Pfeil, B., Landa, C. S., Metzl, N., O'Brien, K. M., Olsen, A., Smith, K., Cosca, C., Harasawa, S., Jones, S. D., Nakaoka, S., Nojiri, Y., Schuster, U., Steinhoff, T., Sweeney, C., Takahashi, T., Tilbrook, B., Wada, C., Wanninkhof, R., Alin, S. R., Balestrini, C. F., Barbero, L., Bates, N. R., Bianchi, A. A., Bonou, F., Boutin, J., Bozec, Y., Burger, E. F., Cai, W.-J., Castle, R. D., Chen, L., Chierici, M., Currie, K., Evans, W., Featherstone, C., Feely, R. A., Fransson, A., Goyet, C., Greenwood, N., Gregor, L., Hankin, S., Hardman-Mountford, N. J., Harlay, J., Hauck, J., Hoppema, M., Humphreys, M. P., Hunt, C. W., Huss, B., Ibánhez, J. S. P., Johannessen, T., Keeling, R., Kitidis, V., Körtzinger, A., Kozyr, A., Krasakopoulou, E., Kuwata, A., Landschützer, P., Lauvset, S. K., Lefèvre, N., Lo Monaco, C., Manke, A., Mathis, J. T., Merlivat, L., Millero, F. J., Monteiro, P. M. S., Munro, D. R., Murata, A., Newberger, T., Omar, A. M., Ono, T., Paterson, K., Pearce, D., Pierrot, D., Robbins, L. L., Saito, S., Salisbury, J., Schlitzer, R., Schneider, B., Schweitzer, R., Sieger, R., Skjelvan, I., Sullivan, K. F., Sutherland, S. C., Sutton, A. J., Tadokoro, K., Telszewski, M., Tuma, M., van Heuven, S. M. A. C., Vandemark, D., Ward, B., Watson, A. J., and Xu, S.: A multi-decade record of high-quality fCO_2 data in version 3 of the Surface Ocean CO_2 Atlas (SOCAT), Earth System Science Data, 8, 383–413, https://doi.org/10.5194/essd-8-383-2016, https://essd.copernicus.org/articles/8/383/2016/, 2016.

Bennington, V., Gloege, L., and McKinley, G. A.: Variability in the Global Ocean Carbon Sink From 1959 to 2020 by Correcting Models With Observations, Geophysical Research Letters, 49, e2022GL098 632, https://doi.org/10.1029/2022GL098632, https://agupubs.onlinelibrary.wiley.com/doi/abs/10.1029/2022GL098632, e2022GL098632 2022GL098632, 2022.

Berthet, S., Séférian, R., Bricaud, C., Chevallier, M., Voldoire, A., and Ethé, C.: Evaluation of an Online Grid-Coarsening Algorithm in a Global Eddy-Admitting Ocean Biogeochemical Model, Journal of Advances in Modeling Earth Systems, 11, 1759–1783, https://doi.org/10.1029/2019MS001644, https://doi.org/10.1029/2019MS001644, 2019.

Bjerknes, J.: A possible response of the atmospheric Hadley circulation to equatorial anomalies of ocean temperature, Tellus, 18, 820–829, https://doi.org/10.3402/tellusa.v18i4.9712, 1966.

Bromwich, D. H. and Fogt, R. L.: Strong Trends in the Skill of the ERA-40 and NCEP–NCAR Reanalyses in the High and Midlatitudes of the Southern Hemisphere, 1958–2001*, Journal of Climate, 17, 4603–4619, ISSN 0894-8755, https://doi.org/10.1175/3241.1, 2004.

Canadell, J. G., Ciais, P., Gurney, K., Le Quéré, C., Piao, S., Raupach, M. R., and Sabine, C. L.: An International Effort to Quantify Regional Carbon Fluxes, Eos, Transactions American Geophysical Union, 92, 81–82, https://doi.org/10.1029/2011EO100001, 2011.

Carroll, D., Menemenlis, D., Dutkiewicz, S., Lauderdale, J. M., Adkins, J. F., Bowman, K. W., Brix, H., Fenty, I., Gierach, M. M., Hill, C., Jahn, O., Landschützer, P., Manizza, M., Mazloff, M. R., Miller, C. E., Schimel, D. S., Verdy, A., Whitt, D. B., and Zhang, H.: Attribution of Space-Time Variability in Global-Ocean Dissolved Inorganic Carbon, Global Biogeochemical Cycles, 36, e2021GB007 162, https://doi.org/10.1029/2021GB007162, https://agupubs.onlinelibrary.wiley.com/doi/abs/10.1029/2021GB007162, e2021GB007162 2021GB007162, 2022.

https://doi.org/10.5194/egusphere-2026-3104
Preprint. Discussion started: 18 June 2026

Crisp, D., Dolman, H., Tanhua, T., McKinley, G. A., Hauck, J., Bastos, A., Sitch, S., Eggleston, S., and Aich, V.: How Well Do We Understand the Land-Ocean-Atmosphere Carbon Cycle?, Reviews of Geophysics, 60, e2021RG000 736, https://doi.org/10.1029/2021RG000736, e2021RG000736 2021RG000736, 2022.

Denvil-Sommer, A., Gehlen, M., Vrac, M., and Mejia, C.: LSCE-FFNN-v1: a two-step neural network model for the reconstruction of surface ocean pCO_2 over the global ocean, Geoscientific Model Development, 12, 2091–2105, https://doi.org/10.5194/gmd-12-2091-2019, https://gmd.copernicus.org/articles/12/2091/2019/, 2019.

Deser, C., Phillips, A., Bourdette, V., and Teng, H.: Uncertainty in climate change projections: the role of internal variability, Climate dynamics, 38, 527–546, https://doi.org/10.1007/s00382-010-0977-x, 2012a.

Deser, C., Phillips, A. S., Tomas, R. A., Okumura, Y. M., Alexander, M. A., Capotondi, A., Scott, J. D., Kwon, Y.-O., and Ohba, M.: ENSO and Pacific Decadal Variability in the Community Climate System Model Version 4, Journal of Climate, 25, 2622 – 2651, https://doi.org/10.1175/JCLI-D-11-00301.1, https://journals.ametsoc.org/view/journals/clim/25/8/jcli-d-11-00301.1.xml, 2012b.

DeVries, T., Holzer, M., and Primeau, F.: Recent increase in oceanic carbon uptake driven by weaker upper-ocean overturning, Nature, 542, 215–218, https://doi.org/10.1038/nature21068, 2017.

DeVries, T., Le Quéré, C., Andrews, O., Berthet, S., Hauck, J., Ilyina, T., Landschützer, P., Lenton, A., Lima, I. D., Nowicki, M., et al.: Decadal trends in the ocean carbon sink, Proceedings of the National Academy of Sciences, 116, 11 646–11 651, https://doi.org/10.1073/pnas.1900371116, 2019.

Di Lorenzo, E., Xu, T., Zhao, Y., Newman, M., Capotondi, A., Stevenson, S., Amaya, D., Anderson, B., Ding, R., Furtado, J., Joh, Y., Liguori, G., Lou, J., Miller, A., Navarra, G., Schneider, N., Vimont, D., Wu, S., and Zhang, H.: Modes and Mechanisms of Pacific Decadal-Scale Variability, Annual Review of Marine Science, 15, 249–275, https://doi.org/10.1146/annurev-marine-040422-084555, 2023.

Doney, S. C., Lima, I., Feely, R. A., Glover, D. M., Lindsay, K., Mahowald, N., Moore, J. K., and Wanninkhof, R.: Mechanisms governing interannual variability in upper-ocean inorganic carbon system and air-sea CO_2 fluxes: Physical climate and atmospheric dust, Deep Sea Research Part II: Topical Studies in Oceanography, 56, 640–655, ISSN 0967-0645, https://doi.org/10.1016/j.dsr2.2008.12.006, surface Ocean CO2 Variability and Vulnerabilities, 2009.

Dong, Y., Bakker, D. C. E., and Landschützer, P.: Accuracy of Ocean CO2 Uptake Estimates at a Risk by a Reduction in the Data Collection, Geophysical Research Letters, 51, ISSN 0094-8276, https://doi.org/10.1029/2024gl108502, 2024.

Eddebbar, Y. A., Rodgers, K. B., Long, M. C., Subramanian, A. C., Xie, S.-P., and Keeling, R. F.: El Niño–Like Physical and Biogeochemical Ocean Response to Tropical Eruptions, Journal of Climate, 32, 2627 – 2649, https://doi.org/10.1175/JCLI-D-18-0458.1, https://journals.ametsoc.org/view/journals/clim/32/9/jcli-d-18-0458.1.xml, 2019.

Fassbender, A. J., Sabine, C. L., Cronin, M. F., and Sutton, A. J.: Mixed-layer carbon cycling at the Kuroshio Extension Observatory, Global Biogeochemical Cycles, 31, 272–288, https://doi.org/10.1002/2016GB005547, https://agupubs.onlinelibrary.wiley.com/doi/abs/10.1002/2016GB005547, 2017.

Fay, A. R., McKinley, G. A., and Lovenduski, N. S.: Southern Ocean carbon trends: Sensitivity to methods, Geophysical Research Letters, 41, 6833–6840, https://doi.org/10.1002/2014GL061324, https://agupubs.onlinelibrary.wiley.com/doi/abs/10.1002/2014GL061324, 2014.

Fay, A. R., Gregor, L., Landschützer, P., McKinley, G. A., Gruber, N., Gehlen, M., Iida, Y., Laruelle, G. G., Rödenbeck, C., Roobaert, A., and Zeng, J.: SeaFlux: harmonization of air–sea CO_2 fluxes from surface pCO_2 data products using a standardized approach, Earth System Science Data, 13, 4693–4710, https://doi.org/10.5194/essd-13-4693-2021, 2021.

Fay, A. R., McKinley, G. A., Lovenduski, N. S., Eddebbar, Y., Levy, M. N., Long, M. C., Olivarez, H. C., and Rustagi, R. R.: Immediate and Long-Lasting Impacts of the Mt. Pinatubo Eruption on Ocean Oxygen and Carbon Inventories, Global Biogeochemical Cycles,

https://doi.org/10.5194/egusphere-2026-3104
Preprint. Discussion started: 18 June 2026

37, e2022GB007 513, https://doi.org/10.1029/2022GB007513, https://agupubs.onlinelibrary.wiley.com/doi/abs/10.1029/2022GB007513, e2022GB007513 2022GB007513, 2023.

Fay, A. R., Carroll, D., McKinley, G. A., Menemenlis, D., and Zhang, H.: Scale-Dependent Drivers of Air-Sea CO2 Flux Variability, Geophysical Research Letters, 51, ISSN 0094-8276, https://doi.org/10.1029/2024gl111911, 2024.

Fay, A. R., Heimdal, T. H., Acquaviva, V., Shaum, A. P., and McKinley, G. A.: Sensitivity of Ocean Carbon Sink Estimates to Rare Observations, Geophysical Research Letters, 52, e2025GL117 961, https://doi.org/https://doi.org/10.1029/2025GL117961, https://agupubs.onlinelibrary.wiley.com/doi/abs/10.1029/2025GL117961, e2025GL117961 2025GL117961, 2025.

Feely, R. A., Wanninkhof, R., Takahashi, T., and Tans, P.: Influence of El Niño on the equatorial Pacific contribution to atmospheric CO_2 accumulation, Nature, 398, 597–601, https://doi.org/10.1038/19273, 1999.

Feely, R. A., Takahashi, T., Wanninkhof, R., McPhaden, M. J., Cosca, C. E., Sutherland, S. C., and Carr, M.-E.: Decadal variability of the air-sea CO_2 fluxes in the equatorial Pacific Ocean, Journal of Geophysical Research: Oceans, 111, https://doi.org/10.1029/2005JC003129, 2006.

Friedlingstein, P., O'Sullivan, M., Jones, M. W., Andrew, R. M., Hauck, J., Olsen, A., Peters, G. P., Peters, W., Pongratz, J., Sitch, S., Le Quéré, C., Canadell, J. G., Ciais, P., Jackson, R. B., Alin, S., Aragão, L. E. O. C., Arneth, A., Arora, V., Bates, N. R., Becker, M., Benoit-Cattin, A., Bittig, H. C., Bopp, L., Bultan, S., Chandra, N., Chevallier, F., Chini, L. P., Evans, W., Florentie, L., Forster, P. M., Gasser, T., Gehlen, M., Gilfillan, D., Gkritzalis, T., Gregor, L., Gruber, N., Harris, I., Hartung, K., Haverd, V., Houghton, R. A., Ilyina, T., Jain, A. K., Joetzjer, E., Kadono, K., Kato, E., Kitidis, V., Korsbakken, J. I., Landschützer, P., Lefèvre, N., Lenton, A., Lienert, S., Liu, Z., Lombardozzi, D., Marland, G., Metzl, N., Munro, D. R., Nabel, J. E. M. S., Nakaoka, S.-I., Niwa, Y., O'Brien, K., Ono, T., Palmer, P. I., Pierrot, D., Poulter, B., Resplandy, L., Robertson, E., Rödenbeck, C., Schwinger, J., Séférian, R., Skjelvan, I., Smith, A. J. P., Sutton, A. J., Tanhua, T., Tans, P. P., Tian, H., Tilbrook, B., van der Werf, G., Vuichard, N., Walker, A. P., Wanninkhof, R., Watson, A. J., Willis, D., Wiltshire, A. J., Yuan, W., Yue, X., and Zaehle, S.: Global Carbon Budget 2020, Earth System Science Data, 12, 3269–3340, https://doi.org/10.5194/essd-12-3269-2020, https://essd.copernicus.org/articles/12/3269/2020/, 2020.

Friedlingstein, P., O'Sullivan, M., Jones, M. W., Andrew, R. M., Bakker, D. C. E., Hauck, J., Landschützer, P., Le Quéré, C., Li, H., Luijkx, I. T., Peters, G. P., Peters, W., Pongratz, J., Schwingshackl, C., Sitch, S., Canadell, J. G., Ciais, P., Aas, K., Alin, S. R., Anthoni, P., Barbero, L., Bates, N. R., Bellouin, N., Benoit-Cattin, A., Berghoff, C. F., Bernardello, R., Bopp, L., Brasika, I. B. M., Chamberlain, M. A., Chandra, N., Chevallier, F., Chini, L. P., Collier, N. O., Colligan, T. H., Cronin, M., Djeutchouang, L., Dou, X., Enright, M. P., Enyo, K., Erb, M., Evans, W., Feely, R. A., Feng, L., Ford, D. J., Foster, A., Fransner, F., Gasser, T., Gehlen, M., Gkritzalis, T., Souza, J. G. D., Grassi, G., Gregor, L., Gruber, N., Guenet, B., Gürses, O., Harrington, K., Harris, I., Heinke, J., Hurtt, G. C., Iida, Y., Ilyina, T., Ito, A., Jacobson, A. R., Jain, A. K., Jarníková, T., Jersild, A., Jiang, F., Jones, S. D., Kato, E., Keeling, R. F., Goldewijk, K. K., Knauer, J., Kong, Y., Korsbakken, J. I., Koven, C., Kunimitsu, T., Lan, X., Liu, J., Liu, Z., Liu, Z., Monaco, C. L., Ma, L., Marland, G., McGuire, P. C., McKinley, G. A., Melton, J., Monacci, N., Monier, E., Morgan, E. J., Munro, D. R., Müller, J. D., Nakaoka, S.-I., Nayagam, L. R., Niwa, Y., Nutzel, T., Olsen, A., Omar, A. M., Pan, N., Pandey, S., Pierrot, D., Qin, Z., Regnier, P. A. G., Rehder, G., Resplandy, L., Roobaert, A., Rosan, T. M., Rödenbeck, C., Schwinger, J., Skjelvan, I., Smallman, T. L., Spada, V., Sreeush, M. G., Sun, Q., Sutton, A. J., Sweeney, C., Swingedouw, D., Séférian, R., Takao, S., Tatebe, H., Tian, H., Tian, X., Tilbrook, B., Tsujino, H., Tubiello, F., Ooijen, E. v., Werf, G. v. d., Velde, S. J. v. d., Walker, A., Wanninkhof, R., Yang, X., Yuan, W., Yue, X., and Zeng, J.: Global Carbon Budget 2025, Earth System Science Data Discussions, 2025, 1–139, https://doi.org/10.5194/essd-2025-659, 2025.

https://doi.org/10.5194/egusphere-2026-3104
Preprint. Discussion started: 18 June 2026

Garreaud, R. D. and Battisti, D. S.: Interannual (ENSO) and Interdecadal (ENSO-like) Variability in the Southern Hemisphere Tropospheric Circulation, Journal of Climate, 12, 2113 – 2123, https://doi.org/10.1175/1520-0442(1999)012<2113:IEAIEL>2.0.CO;2, https://journals.ametsoc.org/view/journals/clim/12/7/1520-0442_1999_012_2113_ieaiel_2.0.co_2.xml, 1999.

Gerber, E. P. and Son, S.-W.: Quantifying the Summertime Response of the Austral Jet Stream and Hadley Cell to Stratospheric Ozone and Greenhouse Gases, Journal of Climate, 27, 5538 – 5559, https://doi.org/10.1175/JCLI-D-13-00539.1, https://journals.ametsoc.org/view/journals/clim/27/14/jcli-d-13-00539.1.xml, 2014.

Gloege, L., McKinley, G. A., Landschützer, P., Fay, A. R., Frölicher, T. L., Fyfe, J. C., Ilyina, T., Jones, S., Lovenduski, N. S., Rodgers, K. B., Schlunegger, S., and Takano, Y.: Quantifying Errors in Observationally Based Estimates of Ocean Carbon Sink Variability, Global Biogeochemical Cycles, 35, e2020GB006 788, https://doi.org/10.1029/2020GB006788, 2021.

Gloege, L., Yan, M., Zheng, T., and McKinley, G. A.: Improved Quantification of Ocean Carbon Uptake by Using Machine Learning to Merge Global Models and pCO_2 Data, Journal of Advances in Modeling Earth Systems, 14, e2021MS002 620, https://doi.org/10.1029/2021MS002620, https://agupubs.onlinelibrary.wiley.com/doi/abs/10.1029/2021MS002620, e2021MS002620 2021MS002620, 2022.

Goyal, R., Sen Gupta, A., Jucker, M., and England, M. H.: Historical and Projected Changes in the Southern Hemisphere Surface Westerlies, Geophysical Research Letters, 48, e2020GL090 849, https://doi.org/10.1029/2020GL090849, https://agupubs.onlinelibrary.wiley.com/doi/abs/10.1029/2020GL090849, e2020GL090849 2020GL090849, 2021.

Gregor, L., Lebehot, A. D., Kok, S., and Scheel Monteiro, P. M.: A comparative assessment of the uncertainties of global surface ocean CO_2 estimates using a machine-learning ensemble (CSIR-ML6 version 2019a) - have we hit the wall?, Geoscientific Model Development, 12, 5113–5136, https://doi.org/10.5194/gmd-12-5113-2019, https://gmd.copernicus.org/articles/12/5113/2019/, 2019.

Gruber, N., Landschützer, P., and Lovenduski, N. S.: The Variable Southern Ocean Carbon Sink, Annual Review of Marine Science, 11, 159–186, https://doi.org/10.1146/annurev-marine-121916-063407, pMID: 30212259, 2019.

Gruber, N., Bakker, D., DeVries, T., Gregor, L., Hauck, J., Landschützer, P., McKinley, G., and Müller, J.: Trends and variability in the ocean carbon sink, Nature Reviews Earth and Environment, 4, 119–134, ISSN 2662-138X, https://doi.org/10.3929/ethz-b-000595538, 2023.

Gürses, Ö., Oziel, L., Karakuş, O., Sidorenko, D., Völker, C., Ye, Y., Zeising, M., Butzin, M., and Hauck, J.: Ocean biogeochemistry in the coupled ocean–sea ice–biogeochemistry model FESOM2.1–REcoM3, Geoscientific Model Development, 16, 4883–4936, https://doi.org/10.5194/gmd-16-4883-2023, https://doi.org/10.5194/gmd-16-4883-2023, 2023.

Hauck, J., Zeising, M., Le Quéré, C., Gruber, N., Bakker, D. C. E., Bopp, L., Chau, T. T. T., Gürses, O., Ilyina, T., Landschützer, P., Lenton, A., Resplandy, L., Rödenbeck, C., Schwinger, J., and Séférian, R.: Consistency and Challenges in the Ocean Carbon Sink Estimate for the Global Carbon Budget, Frontiers in Marine Science, 7, ISSN 2296-7745, https://doi.org/10.3389/fmars.2020.571720, https://www.frontiersin.org/articles/10.3389/fmars.2020.571720, 2020.

Hauck, J., Nissen, C., Landschützer, P., Rodenbeck, C., Bushinsky, S., and Olsen, A.: Sparse observations induce large biases in estimates of the global ocean CO2 sink: an ocean model subsampling experiment, Philosophical Transactions of the Royal Society A, 381, 20220 063, ISSN 1364-503X, https://doi.org/10.1098/rsta.2022.0063, 2023.

Heidemann, H., Cowan, T., Power, S. B., and Henley, B. J.: Statistical relationships between the Interdecadal Pacific Oscillation and El Niño-Southern Oscillation, Climate Dynamics, 2024.

Heimdal, T. H. and McKinley, G. A.: The importance of adding unbiased Argo observations to the ocean carbon observing system, Scientific Reports, 14, 19 763, https://doi.org/10.1038/s41598-024-70617-x, 2024.

https://doi.org/10.5194/egusphere-2026-3104
Preprint. Discussion started: 18 June 2026

Heimdal, T. H., McKinley, G. A., Sutton, A. J., Fay, A. R., and Gloege, L.: Assessing improvements in global ocean pCO2 machine learning reconstructions with Southern Ocean autonomous sampling, Biogeosciences, 21, 2159–2176, https://doi.org/10.5194/bg-21-2159-2024, 2024.

Henley, B. J., Gergis, J., Karoly, D. J., Power, S., Kennedy, J., and Folland, C. K.: A Tripole Index for the Interdecadal Pacific Oscillation, Climate Dynamics, 45, 3077–3090, https://doi.org/10.1007/s00382-015-2525-1, 2015.

Hersbach, H., Bell, B., Berrisford, P., Biavati, G., Horányi, A., Muñoz Sabater, J., Nicolas, J., Peubey, C., Radu, R., Rozum, I., Schepers, D., Simmons, A., Soci, C., Dee, D., and Thépaut, J.-N.: ERA5 monthly averaged data on single levels from 1940 to present. [Dataset], https://doi.org/10.24381/cds.f17050d7, 2023.

Huang, B., Thorne, P. W., Banzon, V. F., Boyer, T., Chepurin, G., Lawrimore, J. H., Menne, M. J., Smith, T. M., Vose, R. S., and Zhang, H.-M.: Extended Reconstructed Sea Surface Temperature, Version 5 (ERSSTv5): Upgrades, Validations, and Intercomparisons, Journal of Climate, 30, 8179 – 8205, https://doi.org/10.1175/JCLI-D-16-0836.1, https://journals.ametsoc.org/view/journals/clim/30/20/jcli-d-16-0836.1.xml, 2017.

Huang, Y., Fassbender, A., and Bushinsky, S.: Biogenic carbon pool production maintains the Southern Ocean carbon sink, Proceedings of the National Academy of Sciences, 120, e2217909 120, https://doi.org/10.1073/pnas.2217909120, https://www.pnas.org/doi/abs/10.1073/pnas.2217909120, 2023.

Ishii, M., Feely, R. A., Rodgers, K. B., Park, G.-H., Wanninkhof, R., Sasano, D., Sugimoto, H., Cosca, C. E., Nakaoka, S., Telszewski, M., Nojiri, Y., Mikaloff Fletcher, S. E., Niwa, Y., Patra, P. K., Valsala, V., Nakano, H., Lima, I., Doney, S. C., Buitenhuis, E. T., Aumont, O., Dunne, J. P., Lenton, A., and Takahashi, T.: Air–sea CO_2 flux in the Pacific Ocean for the period 1990-2009, Biogeosciences, 11, 709–734, https://doi.org/10.5194/bg-11-709-2014, https://bg.copernicus.org/articles/11/709/2014/, 2014.

Jacobson, T. W. and Seager, R.: Pacific Decadal Variability and Its Hydroclimate Teleconnections in CMIP6 Models, Journal of Climate, 38, 5103–5127, https://doi.org/10.1175/JCLI-D-24-0616.1, 2025.

Jiang, F., Seager, R., and Cane, M. A.: A climate change signal in the tropical Pacific emerges from decadal variability, Nature Communications, 15, 8291, https://doi.org/10.1038/s41467-024-52731-6, 2024.

Kang, J. M., Shaw, T. A., Kang, S. M., Simpson, I. R., and Yu, Y.: Revisiting the reanalysis-model discrepancy in Southern Hemisphere winter storm track trends, npj Climate and Atmospheric Science, 7, 252, https://doi.org/10.1038/s41612-024-00801-3, 2024.

Kang, J. M., Thomas, R., Dunstone, N., Shaw, T. A., and Woollings, T.: Robust impact of tropical Pacific SST trends on global and regional circulation in boreal winter, npj Climate and Atmospheric Science, 8, 315, https://doi.org/10.1038/s41612-025-01192-9, 2025.

Keeling, R. and Keeling, C.: Scripps CO2 Program Data [Dataset], https://doi.org/10.6075/J0542KSG, 2017.

Lacroix, F., Ilyina, T., Mathis, M., Laruelle, G. G., and Regnier, P.: Historical increases in land-derived nutrient inputs may alleviate effects of a changing physical climate on the oceanic carbon cycle, Global Change Biology, 27, 5491–5513, https://doi.org/10.1111/gcb.15822, https://doi.org/10.1111/gcb.15822, 2021.

Lan, X., Tans, P., and Thoning, K.: Trends in globally-averaged CO_2 determined from NOAA Global Monitoring Laboratory measurements. [Dataset] National Oceanic and Atmospheric Administration, Earth System Research Laboratory (NOAA/ESRL), https://doi.org/10.15138/9N0H-ZH07, version 2023-04, 2023.

Lan, X., Tans, P., Thoning, K., and NOAA Global Monitoring Laboratory: NOAA Greenhouse Gas Marine Boundary Layer Reference - CO2, https://doi.org/10.15138/DVNP-F961, https://doi.org/10.15138/DVNP-F961, data set, accessed August 30, 2025, 2025.

https://doi.org/10.5194/egusphere-2026-3104
Preprint. Discussion started: 18 June 2026

Landschützer, P., Gruber, N., Haumann, F. A., Rödenbeck, C., Bakker, D. C., Van Heuven, S., Hoppema, M., Metzl, N., Sweeney, C., Takahashi, T., et al.: The reinvigoration of the Southern Ocean carbon sink, Science, 349, 1221–1224, https://doi.org/10.1126/science.aab2620, 2015.

Landschützer, P., Gruber, N., and Bakker, D. C. E.: Decadal variations and trends of the global ocean carbon sink, Global Biogeochemical Cycles, 30, 1396–1417, https://doi.org/10.1002/2015GB005359, 2016.

Landschützer, P., Ilyina, T., and Lovenduski, N. S.: Detecting Regional Modes of Variability in Observation-Based Surface Ocean pCO_2, Geophysical Research Letters, 46, 2670–2679, https://doi.org/10.1029/2018GL081756, 2019.

Law, R. M., Ziehn, T., Matear, R. J., Lenton, A., Chamberlain, M. A., Stevens, L. E., Wang, Y.-P., Srbinovsky, J., Bi, D., Yan, H., and Vohralik, P. F.: The carbon cycle in the Australian Community Climate and Earth System Simulator (ACCESS-ESM1) – Part 1: Model description and pre-industrial simulation, Geoscientific Model Development, 10, 2567–2590, https://doi.org/10.5194/gmd-10-2567-2017, https://doi.org/10.5194/gmd-10-2567-2017, 2017.

Le Quéré, C., Rödenbeck, C., Buitenhuis, E. T., Conway, T. J., Langenfelds, R., Gomez, A., Labuschagne, C., Ramonet, M., Nakazawa, T., Metzl, N., Gillett, N., and Heimann, M.: Saturation of the Southern Ocean CO_2 Sink Due to Recent Climate Change, Science, 316, 1735–1738, https://doi.org/10.1126/science.1136188, https://www.science.org/doi/abs/10.1126/science.1136188, 2007.

Levy, M., Bopp, L., Karleskind, P., Resplandy, L., Ethe, C., and Pinsard, F.: Physical pathways for carbon transfers between the surface mixed layer and the ocean interior, Global Biogeochemical Cycles, 27, 1001–1012, https://doi.org/10.1002/gbc.20092, https://agupubs.onlinelibrary.wiley.com/doi/abs/10.1002/gbc.20092, 2013.

Li, Q. and England, M. H.: Tropical Indo-Pacific Teleconnections to Southern Ocean Mixed Layer Variability, Geophysical Research Letters, 47, e2020GL088 466, https://doi.org/10.1029/2020GL088466, https://agupubs.onlinelibrary.wiley.com/doi/abs/10.1029/2020GL088466, e2020GL088466 10.1029/2020GL088466, 2020.

Lovenduski, N. S., Swart, N. C., Sutton, A. J., Fyfe, J. C., McKinley, G. A., Sabine, C., and Williams, N. L.: The Ocean Carbon Response to COVID-Related Emissions Reductions, Geophysical Research Letters, 48, e2020GL092 263, ISSN 0094-8276, https://doi.org/10.1029/2020gl092263, 2021.

Mantua, N. J. and Hare, S. R.: The Pacific Decadal Oscillation, Journal of oceanography, 58, 35–44, https://doi.org/10.1023/A:1015820616384, 2002.

Mayot, N., Le Quéré, C., Rödenbeck, C., Bernardello, R., Bopp, L., Djeutchouang, L. M., Gehlen, M., Gregor, L., Gruber, N., Hauck, J., Iida, Y., Ilyina, T., Keeling, R. F., Landschützer, P., Manning, A. C., Patara, L., Resplandy, L., Schwinger, J., Séférian, R., Watson, A. J., Wright, R. M., and Zeng, J.: Climate-driven variability of the Southern Ocean CO_2 sink, Philosophical Transactions of the Royal Society A: Mathematical, Physical and Engineering Sciences, 381, 20220 055, https://doi.org/10.1098/rsta.2022.0055, 2023.

McKinley, G. A., Follows, M. J., and Marshall, J.: Mechanisms of air-sea CO_2 flux variability in the equatorial Pacific and the North Atlantic, Global Biogeochemical Cycles, 18, GB2011, https://doi.org/10.1029/2003GB002179, 2004.

McKinley, G. A., Fay, A. R., Eddebbar, Y. A., Gloege, L., and Lovenduski, N. S.: External Forcing Explains Recent Decadal Variability of the Ocean Carbon Sink, AGU Advances, 1, e2019AV000 149, https://doi.org/10.1029/2019AV000149, https://agupubs.onlinelibrary.wiley.com/doi/abs/10.1029/2019AV000149, e2019AV000149 2019AV000149, 2020.

Mikaloff Fletcher, S. E., Gruber, N., Jacobson, A. R., Doney, S. C., Dutkiewicz, S., Gerber, M., Follows, M., Joos, F., Lindsay, K., Menemenlis, D., Mouchet, A., Müller, S. A., and Sarmiento, J. L.: Inverse estimates of anthropogenic CO_2 uptake, transport, and storage by the ocean, Global Biogeochemical Cycles, 20, https://doi.org/10.1029/2005GB002530, https://agupubs.onlinelibrary.wiley.com/doi/abs/10.1029/2005GB002530, 2006.

https://doi.org/10.5194/egusphere-2026-3104
Preprint. Discussion started: 18 June 2026

Müller, J. D., Gruber, N., Carter, B., Feely, R., Ishii, M., Lange, N., Lauvset, S. K., Murata, A., Olsen, A., Pérez, F. F., Sabine, C., Tanhua, T., Wanninkhof, R., and Zhu, D.: Decadal Trends in the Oceanic Storage of Anthropogenic Carbon From 1994 to 2014, AGU Advances, 4, ISSN 2576-604X, https://doi.org/10.1029/2023av000875, 2023.

Newman, M., Alexander, M. A., Ault, T. R., Cobb, K. M., Deser, C., Lorenzo, E. D., Mantua, N. J., Miller, A. J., Minobe, S., Nakamura, H., Schneider, N., Vimont, D. J., Phillips, A. S., Scott, J. D., and Smith, C. A.: The Pacific Decadal Oscillation, Revisited, Journal of Climate, 29, 4399 – 4427, https://doi.org/10.1175/JCLI-D-15-0508.1, https://journals.ametsoc.org/view/journals/clim/29/12/jcli-d-15-0508.1.xml, 2016.

Peters, G. P., Le Quéré, C., Andrew, R. M., Canadell, J. G., Friedlingstein, P., Ilyina, T., Jackson, R. B., Joos, F., Korsbakken, J. I., McKinley, G. A., et al.: Towards real-time verification of CO_2 emissions, Nature Climate Change, 7, 848–850, https://doi.org/10.1038/s41558-017-0013-9, 2017.

Pezza, A. B., Simmonds, I., and Renwick, J. A.: Southern hemisphere cyclones and anticyclones: recent trends and links with decadal variability in the Pacific Ocean, International Journal of Climatology, 27, 1403–1419, https://doi.org/10.1002/joc.1477, https://rmets.onlinelibrary.wiley.com/doi/abs/10.1002/joc.1477, 2007.

Power, S., Casey, T., Folland, C., Colman, A., and Mehta, V.: Inter-decadal modulation of the impact of ENSO on Australia, Climate Dynamics, 15, 319–324, https://doi.org/10.1007/s003820050284, 1999.

Resplandy, L., Séférian, R., and Bopp, L.: Natural variability of CO_2 and O_2 fluxes: What can we learn from centuries-long climate models simulations?, Journal of Geophysical Research: Oceans, 120, 384–404, https://doi.org/10.1002/2014JC010463, 2015.

Rödenbeck, C., Bakker, D. C. E., Gruber, N., Iida, Y., Jacobson, A. R., Jones, S., Landschützer, P., Metzl, N., Nakaoka, S., Olsen, A., Park, G.-H., Peylin, P., Rodgers, K. B., Sasse, T. P., Schuster, U., Shutler, J. D., Valsala, V., Wanninkhof, R., and Zeng, J.: Data-based estimates of the ocean carbon sink variability - first results of the Surface Ocean pCO_2 Mapping intercomparison (SOCOM), Biogeosciences, 12, 7251–7278, https://doi.org/10.5194/bg-12-7251-2015, https://bg.copernicus.org/articles/12/7251/2015/, 2015.

Sakamoto, K., Nakano, H., Urakawa, S., Toyoda, T., Kawakami, Y., Tsujino, H., and Yamanaka, G.: Reference manual for the Meteorological Research Institute Community Ocean Model version 5 (MRI.COMv5), Technical Report of the Meteorological Research Institute, https://doi.org/10.11483/mritechrepo.87, https://doi.org/10.11483/mritechrepo.87, 2023.

Sallée, J.-B., Speer, K., and Rintoul, S.: Zonally asymmetric response of the Southern Ocean mixed-layer depth to the Southern Annular Mode, Nature Geoscience, 3, 273–279, https://doi.org/10.1038/ngeo812, 2010.

Sauvé, J., Gray, A. R., Prend, C. J., Bushinsky, S. M., and Riser, S. C.: Carbon Outgassing in the Antarctic Circumpolar Current Is Supported by Ekman Transport From the Sea Ice Zone in an Observation-Based Seasonal Mixed-Layer Budget, Journal of Geophysical Research: Oceans, 128, e2023JC019 815, https://doi.org/10.1029/2023JC019815, https://agupubs.onlinelibrary.wiley.com/doi/abs/10.1029/2023JC019815, e2023JC019815 2023JC019815, 2023.

Schwinger, J., Goris, N., Tjiputra, J. F., Kriest, I., Bentsen, M., Bethke, I., Ilicak, M., Assmann, K. M., and Heinze, C.: Evaluation of NorESM-OC (versions 1 and 1.2), the ocean carbon-cycle stand-alone configuration of the Norwegian Earth System Model (NorESM1), Geosci. Model Dev., 9, 2589–2622, https://doi.org/10.5194/gmd-9-2589-2016, 2016.

Séférian, R., Nabat, P., Michou, M., Saint-Martin, D., Voldoire, A., Colin, J., Decharme, B., Delire, C., Berthet, S., Chevallier, M., Sénési, S., Franchisteguy, L., Vial, J., Mallet, M., Joetzjer, E., Geoffroy, O., Guérémy, J.-F., Moine, M.-P., Msadek, R., Ribes, A., Rocher, M., Roehrig, R., Salas-y Mélia, D., Sanchez, E., Terray, L., Valcke, S., Waldman, R., Aumont, O., Bopp, L., Deshayes, J., Éthé, C., and Madec, G.: Evaluation of CNRM Earth System Model, CNRM-ESM2-1: Role of Earth System Processes in Present-Day and Future Climate, Journal

https://doi.org/10.5194/egusphere-2026-3104
Preprint. Discussion started: 18 June 2026

of Advances in Modeling Earth Systems, 11, 4182–4227, https://doi.org/10.1029/2019ms001791, https://doi.org/10.1029/2019ms001791, 2019.

Sexton, D. M. H.: The effect of stratospheric ozone depletion on the phase of the Antarctic Oscillation, Geophysical Research Letters, 28, 3697–3700, https://doi.org/10.1029/2001GL013376, https://agupubs.onlinelibrary.wiley.com/doi/abs/10.1029/2001GL013376, 2001.

Stock, C. A., Dunne, J. P., Luo, J. Y., Ross, A. C., Oostende, N. V., Zadeh, N., Cordero, T. J., Liu, X., and Teng, Y.: Photoacclimation and Photoadaptation Sensitivity in a Global Ocean Ecosystem Model, Journal of Advances in Modeling Earth Systems, 17, ISSN 1942-2466, https://doi.org/10.1029/2024ms004701, 2025.

Tsujino, H., Nakano, H., Sakamoto, K., Urakawa, L. S., Toyama, K., Kosugi, N., Kitamura, Y., Ishii, M., Nishikawa, S., Nishikawa, H., Sugiyama, T., and Ishikawa, Y.: Impact of increased horizontal resolution of an ocean model on carbon circulation in the North Pacific Ocean, Journal of Advances in Modeling Earth Systems, 16, e2023MS003 720, https://doi.org/10.1029/2023MS003720, https://doi.org/10.1029/2023MS003720, 2024.

Wang, G., Cai, W., Santoso, A., Wu, L., Fyfe, J. C., Yeh, S.-W., Ng, B., Yang, K., and McPhaden, M. J.: Future Southern Ocean warming linked to projected ENSO variability, Nature Climate Change, 12, 649–654, https://doi.org/10.1038/s41558-022-01398-2, 2022.

Wanninkhof, R.: Relationship between wind speed and gas exchange over the ocean revisited, Limnology and Oceanography: Methods, 12, 351–362, https://doi.org/10.4319/lom.2014.12.351, 2014.

Wolter, K. and Timlin, M. S.: El Niño/Southern Oscillation behaviour since 1871 as diagnosed in an extended multivariate ENSO index (MEI.ext), International Journal of Climatology, 31, 1074–1087, https://doi.org/10.1002/joc.2336, 2011.

Wong, S. C. K., McKinley, G. A., and Seager, R.: Equatorial Pacific pCO_2 Interannual Variability in CMIP6 Models, Journal of Geophysical Research: Biogeosciences, 127, e2022JG007 243, https://doi.org/10.1029/2022JG007243, https://agupubs.onlinelibrary.wiley.com/doi/abs/10.1029/2022JG007243, e2022JG007243 2022JG007243, 2022.

Wright, R. M., Le Quéré, C., Buitenhuis, E., Pitois, S., and Gibbons, M. J.: Role of jellyfish in the plankton ecosystem revealed using a global ocean biogeochemical model, Biogeosciences, 18, 1291–1320, https://doi.org/10.5194/bg-18-1291-2021, 2021.

Yang, B., Shadwick, E. H., Schultz, C., and Doney, S. C.: Annual Mixed Layer Carbon Budget for the West Antarctic Peninsula Continental Shelf: Insights From Year-Round Mooring Measurements, Journal of Geophysical Research: Oceans, 126, e2020JC016 920, https://doi.org/10.1029/2020JC016920, https://agupubs.onlinelibrary.wiley.com/doi/abs/10.1029/2020JC016920, e2020JC016920 2020JC016920, 2021.

Zhang, T., Hoerling, M. P., Perlwitz, J., and Xu, T.: Forced Atmospheric Teleconnections During 1979–2020, Journal of Climate, 35, 6055–6077, https://doi.org/10.1175/JCLI-D-21-0612.1, 2022.

Zhang, Y., Wallace, J. M., and Battisti, D. S.: ENSO-like Interdecadal Variability: 1900-93, Journal of Climate, 10, 1004–1020, https://doi.org/10.1175/1520-0442(1997)010<1004:ELIV>2.0.CO;2, 1997.

Zuo, H., Balmaseda, M. A., Tietsche, S., Mogensen, K., and Mayer, M.: The ECMWF operational ensemble reanalysis–analysis system for ocean and sea ice: a description of the system and assessment, Ocean Science, 15, 779–808, https://doi.org/10.5194/os-15-779-2019, 2019.